nature portfolio

Peer Review File

Ligand-tuning copper in coordination polymers for efficient electrochemical C–C coupling

REVIEWER COMMENTS

Reviewer #1 (Remarks to the Author):

The authors report about the use of copper-based coordination polymers for electrochemical C–C coupling in CO2RR. The work is well performed with many supporting characterization therefore I suggest acceptance in Nature Communication after addressing some minor comments.

1) The authors report the TEM analysis in the supporting information. It would be interesting the show the elemental maps of copper before and after the electrochemical CO2RR.

2) The authors perform operando XAS at OCP and different voltages showing the formation of Cu-C bond with the disappearance of Cu-O one when the negative potentials are applied. This is attributed to *CO coverage and is very interesting. If this statement is true, the Cu-O bond should reappear when going back to OCP during the operando EXAFS. Could the authors provide those data?

3) Can the authors provide contact angle measurements of the Cu-coordination polymers with the different ligands? This will help to exclude that the difference in the observed results is not due to a difference in the wettability of the catalysts.

4) It can be useful to add a sentence in the conclusions to suggest the readers future direction based on the present discovery.

5) In supplementary Fig.2, it could be beneficial to add the reference pattern of Cu, Cu2O, CuO and Cu-polymer.

Reviewer #2 (Remarks to the Author):

The authors prepare an interesting array of metal-organic Cu-based ligands for CO2RR and connected a change in CO binding strength and product formation. The Cu tuning and its dynamics are currently of great interest (10.1038/s41467-021-26743-5, 10.1038/s41929-023-01070-8). Due to the huge interest and the importance of a persistent structure in this study to assert the authors claims of rational tuning, it is increasingly important for authors to confirm the in operando structure of their material. To assert this, the authors have included a substantial amount of in situ data (e.g. Fig.S13, S15, S17, S20, etc.) However, I have concerns about several aspects of these in situ studies for stability analysis (laid out below) including: technique limitations, reactor/mass transport-based differences in product formation, and unclear analysis.

A lot of the single-site character and material stability was asserted with XAS e.g. “No metallic Cu–Cu bond was identified, suggesting the single-site nature of formed Ln-Cu (Fig. 2d, Supplementary Fig. 5 and Table 1).” And Figure S13 “No metallic Cu patterns existed after CO2RR, indicating the coordination structure of L2-Cu was maintained” However, previous studies: https://pubs.acs.org/doi/full/10.1021/acscatal.3c01116 have indicated that EXAFS is not sensitive enough to assert the single-site nature of a material. Can the authors comment on this in light of this new understanding of EXAFS limitations?

RE: Fig S19: “The weak signals were caused by the interference of ligand molecules existed in the catalysts and lack of localised surface plasmon resonance (LSPR) effect, which is common in metallic Cu-based catalysts” While this does make sense, what is confusing is why you would see in some cases the CO peak go away and come back (e.g. E -0.92 to -1.01) or go away completely (e.g. a, c, d, f). Furthermore, as the authors also note that “COatop species at ~2060 cm-1 was detected on Ln-Cu catalysts, indicating the single-site nature of the catalysts.”, it seems like this decrease could be consistent with restructuring. Can the authors comment on this specifically?

“The resulting Ln-Cu had similar crystal packing (X-ray diffraction (XRD), Fig. S2)” It is nice that they are similar, however the authors should comment on: 1) the structure, what each peak corresponds to (hkl), 2) why the FWMs are different, esp. peak ~ 28deg 2th. Also, a peak at 5deg 2th is very, very low, what does this structurally represent? Also, XRD was not discussed in the methods. Please give details about the characterization, including the source.

The authors state for Fig. S13 that “No metallic Cu patterns existed after CO2RR, indicating the coordination structure of L2-Cu was maintained” However, after CO2RR, none of the features present before catalysis seem to remain e.g. major loss of peak at 10, 15, 28, 32. This seems to indicate huge structural changes. Can the authors comment?

It has been shown that the cell geometry in CO2RR (10.1016/j.electacta.2022.141698, 10.1016/j.joule.2023.05.010) can impact selectivity dramatically. Can the authors confirm that they have similar selectivity in their different in situ cells? If not, can they discuss / explain what that might mean for their interpretations? Also, please note I have typically seen in situ being used to refer to cells that are in aqueous conditions, with applied potential, but do not confirm product formation, while operando measurements confirm product formation. The authors seem to go back and forth (operando XAS, in situ IR/RAMAN) without clarifying.

“Besides, the Raman shifts from 200 cm−1 to 1700 cm−1, typical vibrational modes of Ln-Cu coordination polymers, showed almost no change compared to the spectrum at 1 OCP (Supplementary Fig. 20), which provided complementary evidence of Ln-Cu stability.” This does not seem consistent with my interpretation of the figures, especially between 200 and 500 for B, C, E and F. Furthermore, the authors also say “The peaks at 200–1700 cm- 1 correspond to the vibrational modes of molecular structures in Ln-Cu.”, but offer no insights into which peak correlated with what within the structure. It would be necessary to have more annotations and analysis of such complex data.

Small:

RE: Fig S8, is F also seen in L1 and L3 Ln-Cu catalysts? Furthermore, is this still seen after catalysis?

“The Raman spectra of C≡O stretch in the range of 1900–2200 cm−1 showed a redshift from L1-Cu to L6-Cu, under the same applied potential (Fig. 5e).” Do you also see a shift in the raman peak with applied potentials? I think it would be valuable to do the same analysis for Fig S19 and discuss.

Reviewer #3 (Remarks to the Author):

The authors report on a system of catalysts composed of Cu in PhTA linear/cross-linked coordination network with varying functionality; electron acceptance/donation from functional groups towards Cu is regulated via the conjugated structure of the linkers. Cu2+ sites are coordinated in plane square geometry by 4 ligands: two network linkers into linear chains, and two substitutable electron donors (**OH-, **Cl-) that cross-link the linear chains. CO2RR electrocatalysis is proposed to take place through replacement of the electron donor groups by *(CO)*(CO), proposed via DFT as precursor to C-C coupling. The authors present in detail the synthesis, electrochemical testing and thorough characterization by many analytical methods and DFT.

The central finding is a formulated descriptor eta_{C-C coupling}, describing the efficiency of C-C-coupling as a function of linker functionality and applied potential. Several linear relationships (including a "volcano" plot) are reported between the HOMO level, Bader charge, *CO intermediate bonding at the Cu sites, and eta_{C-C coupling}.

The overall quality of the experiments and conclusions is satisfactory, and has the potential of valuable insights into CO2RR catalysis, especially given the large amount of data presented as evidence. However, the data documentation and treatment must be improved as to not cause false interpretation.

I cannot evaluate the novelty in the application of the PhTA-Cu system for CO2RR due to my limited expertise in this field, but if considered novel enough by fellow reviewers from the electrochemistry community, I recommend acceptance after major revision.

General remarks:

For such a broad-audience journal, reading the paper should be easy and contain sufficient literature references for non-experts. The authors should lead the reader though the many results to concise conclusions. On page 10, after data is presented and the authors arrive at some conclusions, they suddenly start presenting even more data on the Ln-Cu series to derive further conclusions, so I do not know then the paper will finish.

I suggest to re-structure the paper and separate it into 4 blocks (in order that the authors find appropriate): synthesis; all non-operando characeterization of the Ln-Cu series; testing; operando studies.

Specific remarks:

1.

Ln-Cu as a catalyst system can be categorized as a reticular 3D material among other catalyst systems. Please refer to review https://pubs.rsc.org/en/content/articlelanding/2020/CS/D0CS00835D and other work on Cu-based CO2RR-electrocatalysis by B. Roldan Cuenya.

2.

The authors claim to have derived a "volcano plot" for eta_CCcoupling - the term is known from work by J. Nørskov for describing activity as a function of descriptors. Only 1 point on the left side of the "volcano" (L1-Cu) is insufficient, more points are needed to verify the significance. There are already several linear trends derived in this study, and L1-Cu is an outlier in terms of eta_CCcoupling. I would address this trend as "volcano-like due to outlier", focus on the other linear relationships as central finding, and leave space for future studies. Or work with only L2-L6, and place L1-Cu into Supporting Information.

3.

Why do the authors call C2 products C2+? Do they believe that C3 and higher can be produced via the proposed reaction mechanism, analogous to Fischer-Tropsch synthesis? If yes, please explain. If no, call the products C2.

4.

The authors propose *CO to be the key intermediate for C2+ selectivity. Please provide sufficient evidence from literature, including the one mentioned above, for what intermediate is key for CO2RR. E.g. the paper https://pubs.acs.org/doi/10.1021/acs.jpcc.0c10736 assumes *CO as part of the mechanism, but traditionally, non-CO2-based cross-coupling knows many other mechanisms and reactants (see e.g. https://en.wikipedia.org/wiki/Cross-coupling_reaction).

5.

Page 8, Line 17: The HOMO level can be tuned by varying the linker functionality, and this directly correlates towards activity. Can the authors explain this dependency in terms of bonding strength and mechanism?

6.

The quantity eta_CCcoupling is a function of FE, but it is not explained how FE is determined/calculated. Please explain this; apparently it is not straightforward, refer to literature such as https://pubs.acs.org/doi/10.1021/acsenergylett.3c02362 .

7.

XRD:

- Suppl Fig 2: check axis increments, and make them comparable to other XRD data presented in paper and SupplInfo.

- The reflections of Ln-Cu are quite broad. Can the authors add reference lines from database or own refinement for Ln-Cu (at least L2-Cu) to indicate where to expect reflections.

- Suppl Fig 13: the authors claim that no metallic Cu seen. What are the small bumps in the C2-Cu pattern at the position where Cu metal reference lines are located? (for this reason, please give reflection position for Ln-Cu).

- Supp Fig 13 and 17: Comnparisons are made between pure catalysts prior to testing, and catalysts on carbon paper after testing. The comparison is very inconclusive because of the large difference caused by

the carbon paper. Can the authors indicate the important reflections, or compare the catalysts prior to testing also deposited on carbon paper?

8.

The TEM images presented are not HR-TEM; please correct this throughout. Please briefly clarify whether only the sample is visible, or TEM grid material (e.g lacey C) is also visible. Please specify the details of TEM sample preparation and acquisition details in Methods.

9.

FTIR/Raman:

- Please check and compare vibrational speciation of the CO peak, and explicitly mention which wavenumbers are relevant. In Fig 3 (c) (FTIR) and 5 (e) (Raman), the CO peak appears very vague. Please adjust the stacking and scaling such that the peak shape and maximum is clearly visible.

- Fig 5 (d): how are the decay curves "normalized"? An exponential decay cannot go to zero! Please check and correct.

10.

XANES:

- Fig 3 (d): The authors claim that the XANES spectra remain unchanged during reaction at different potentials, and show a stacked plot where no changes are visible. Can the authors show the spectra overlapped to emphasize any minute changes? I would expect some very small variations expecially when different potentials are applied, and the intermediate species are in contact with Cu. Also narrow the plot range to e.g. 8970-9030 eV. to show the spectra in better detail.

- Page 5, Line 17: Please specify "The *local* atomic structure...".

- Fig 2 (c): Please show the detail of the Cu K-pre-edge peak, which is characteristic for Cu2+

11.

EXAFS:

- The presentation and analysis of the EXAFS spectra must be improved significantly, as follows.

- The EXAFS must be presented as FT-EXAFS (magnitude and imaginary part) in the main text and EXAFS in k-space in SuppInfo. The individual curves must be stacked. If fits are included, they are overlapped with the data. See examples in e.g. https://chemistry-europe.onlinelibrary.wiley.com/doi/full/10.1002/cctc.202200573 .

- What do the authors achieve with wavelet transforms? To my knowledge, WTs are used to estimate whether the peaks in FT-EXAFS originate in light elements (correlate with low k) or heavy elements (correlate with high k) - this, together with any other knowledge gained, must be stated. The k-space and R-space spectra used for the WTs must be shown (e.g. in SupplInfo).

- Please mention the k-range and R-range used for fitting.

- When reporting fit results, also S02, sigma2, deltaE0 and R-factor must be stated in the table.

- The authors use a very detailed model for fitting the first coordination shell, with C, N and O as back-scatterers, displaced by small shifts from 2 Å. Further shells are neglected. The first problem is that the three neighboring back-scatterers have very similar scattering factors and are therefore usually not distinguishable - the correct/realistic approach would be to use a single shell Cu-O/N/C an drefine one distance. If several distances are really possible to resolve, a comparison between a fit with 3 distances and a fit with 1 single distance must be made, where the former has a smaller R-factor or chi^2 than the latter. In that case, a path analysis (plotting the individual shells, preferrably as Imaginary part of FT-EXAFS) would be helpful. The second problem is the neglectance of further shells up to 3.5-4.0 Å. Including these shells to the model will significantly justify the use of EXAFS, which is to verify the structure integrity from the point of view of local atomic order.

12.

Suppl Fig 4: Are the Cu LMM spectra - Auger? If so, please mention it. In the caption, "X-Cu" probably means Ln-Cu? Please make this wording consistent.

13.

Page 7 Lines 8-9 and Suppl Fig 12: what catalyst was used for the MEA long-term testing?

14.

Figures in general: Why do the authors only show one structure in the manuscript and the rest in SupplInfo? Please reconsider this, because the reader wants to see data for all the samples mentioned.

15.

Suppl Fig 14: Photo at beamline: please explain what the reader is looking at. Label the main components (ion chambers, fluorence detector, cell, potentiostat, electrolyte flow in/out); draw the X-ray beam path.

16.

The Methods section mentions SEM - is that data shown?

17.

Fig 1 (c): Please invert y-axis for proper orientation.

18.

For the word operando please use italics.

19.

In Methods: incorrectly printed character "-" for inverse units, i.e. mg cm-1, mL min-1, etc.

20.

Page 9 Line 7 and Fig 4 (b): Please use subscripts for molecules FE_{C_{2+}} and FE_{CH_{4}} .

21.

Fig 4 (d): Please use proper label i.e. U = -0.93 +/- 0.01 V (no "@" etc), and use consistent precision (either 2 or 3 decimal places).

22.

Fig 5: please use proper legends/labels in the figures for the curves. The "color scale" is really confusing and illegible in black/white print.

23.

References:

Please use full author list. Include DOI if required.

Response Letter

We thank the editor and all reviewers for the thoughtful and constructive comments, which help us improve the quality of this manuscript. Below we respond to each reviewer's remarks point by point.

Reviewer's comments are in blue and the changes we made in the manuscript are in green.

Reviewer #1:

The authors report about the use of copper-based coordination polymers for electrochemical C–C coupling in CO2RR. The work is well performed with many supporting characterization therefore I suggest acceptance in Nature Communication after addressing some minor comments.

Reply: We sincerely thank the reviewer for the overall evaluation. The point-by-point reply is below.

1. The authors report the TEM analysis in the supporting information. It would be interesting the show the elemental maps of copper before and after the electrochemical CO2RR.

Reply: We have measured, using SEM-EDS mapping, the elemental distribution of **L2**-Cu before and after the electrochemical CO_2RR. Specifically, following the same preparation method as performance tests in the flow cell, **L2**-Cu was spray-coated on the GDE with a nominal loading amount of 0.8 mg cm^{-2}. After testing at 200 mA cm^{-2} for 30 min, the GDE was gently wash with deionised water and dried by an argon flow.

Both maps obtained before and after CO_2RR (Figures R1 & R2, Table R1) demonstrated uniform dispersion of copper in the catalysts.

In the revised manuscript, we updated as below:

Page 5: Scanning electron microscopy energy-dispersive X-ray spectroscopy (SEM-EDS) mapping shows uniform dispersion of N, Cu, and O elements (Supplementary Fig. 5).

Page 7: SEM-EDS mapping demonstrates the uniform disperse of Cu after CO_2RR (Supplementary Fig. 18 and Table 5).

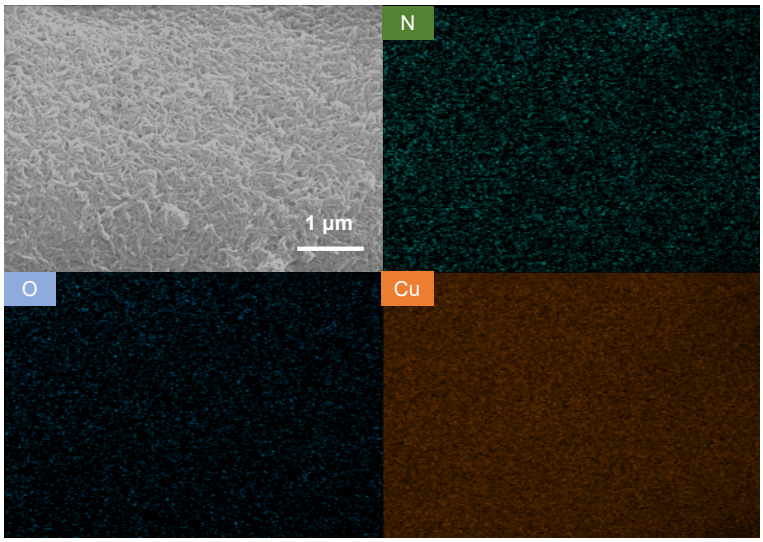

Figure R1 (now added as Supplementary Fig. 5 in SI) | Scanning electron microscopy energy-dispersive X-ray spectroscopy (SEM-EDS) mapping of synthesised L2-Cu, showing the uniform dispersion of Cu, N, and O in the catalyst. **L2**-Cu was spray-coated on the carbon paper.

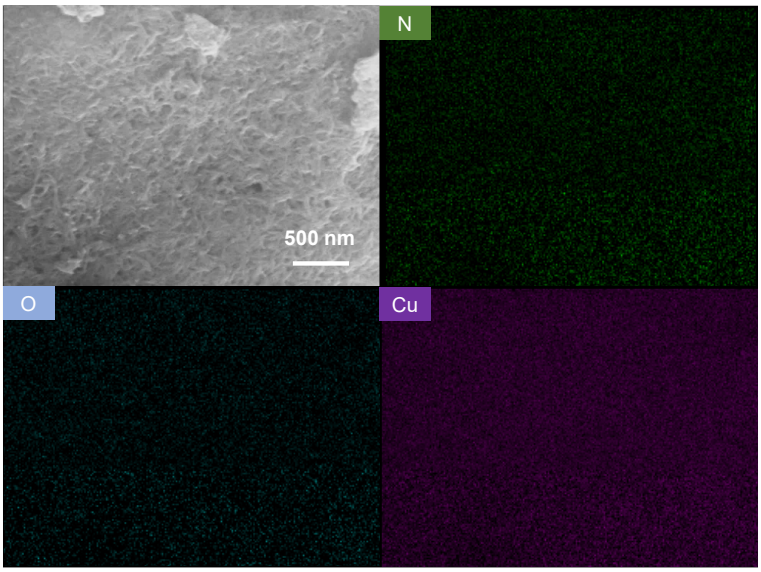

Figure R2 (now added as Supplementary Fig. 18 in SI) | SEM-EDS mapping of L2-Cu following CO_2RR test at 200 mA cm^{-2} for 30 minutes, showing the uniform dispersion of Cu, N, and O in the catalyst after CO_2RR.

Table R1 (now added as Supplementary Table 5 in SI) | The mass percentage of Cu in L2-Cu before and after CO_2RR. The result was determined by SEM-EDS mapping.

Catalyst	Cu (wt. %)[a]
L2-Cu before CO_2RR	29.8
L2-Cu after CO_2RR	29.0

[a]mass percentage.

2. The authors perform *operando* XAS at OCP and different voltages showing the formation of Cu-C bond with the disappearance of Cu-O one when the negative potentials are applied. This is attributed to *CO coverage and is very interesting. If this statement is true, the Cu-O bond should reappear when going back to OCP during the *operando* EXAFS. Could the authors provide those data?

Reply: We have conducted additional *operando* XAS studies of **L2**-Cu (Figure R3) to track the Cu–O bond under applied potentials and at open circuit potential (OCP). The fitting results showed the reappearance of Cu–O bond with a coordination number (CN) of ~2 along with the disappearance of Cu–C bond (Figure R4 and Table R2). Further, FT-EXAFS fitting showed similar local atomic structures of **L2**-Cu before and after reaction.

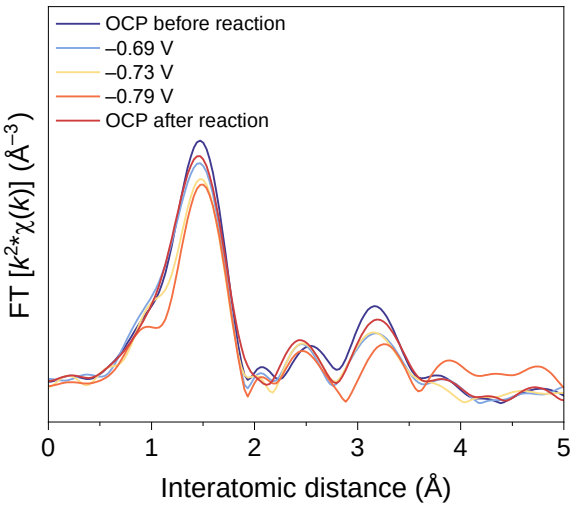

Figure R3 (now added as Supplementary Fig. 25 in SI) | *Operando* Fourier-transform EXAFS spectra for L2-Cu at the Cu *k*-edge.

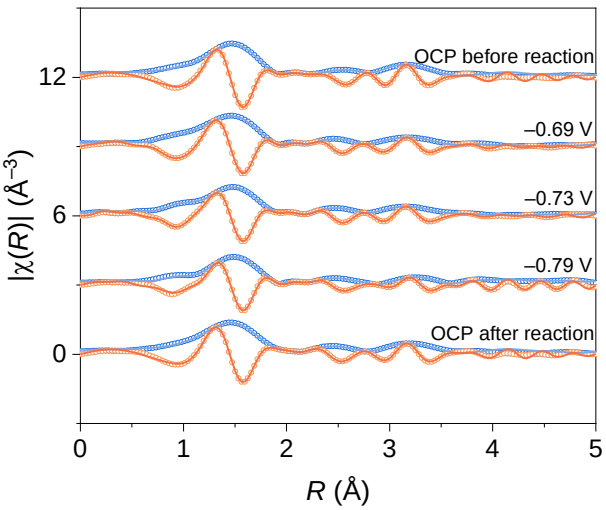

Figure R4 (now added as Supplementary Fig. 26 in SI) | The *operando* Fourier-transform EXAFS spectra (magnitude and imaginary part) for L2-Cu at the Cu *k*-edge, showing the magnitude (experimental data: blue circles; fitting data: blue lines) and imaginary portions (experimental data: orange circles; fitting

data: orange lines;) of Fourier transforms of the data. The *k*-range of 2.5–11 $Å^{-1}$ and the *R*-range of 0–4 Å were used for the fits.

Table R2 (now added as part of Supplementary Tables 1 and 9 in SI) | Interatomic distances and coordination numbers determined by EXAFS analysis of L2-Cu at OCP state before and after CO_2RR. Data rang k = 2.5–11 $Å^{-1}$, amplitude reaction factor S_0^2 = 0.8, bond distance R = 0–4 Å. CN: Coordination numbers. ΔE: The inner potential shift. σ^2: The Debye-Waller factor.

	Scatter path	CN	*R* (Å)	ΔE (eV)	σ^2 ($Å^2$)	R-factor
OCP before reaction	Cu–O	2.00	1.83	1.2	0.00297	0.64%
	Cu–N	2.00	1.99	1.2	0.00604	
OCP after reaction	Cu–O	2.00	1.82	1.2	0.00407	0.57%
	Cu–N	2.00	1.99	1.2	0.00741	

We have now included Figures R3 and R4 in the revised SI.

In the revised manuscript, we updated on page 8: Besides, the CN of Cu–O bond recovered to ~2 with the disappearance of Cu–C bond when the applied potential was reversed to open circuit potential (OCP) state (Supplementary Table 9).

3. Can the authors provide contact angle measurements of the Cu-coordination polymers with the different ligands? This will help to exclude that the difference in the observed results is not due to a difference in the wettability of the catalysts.

Reply: We now provide the wettability information of the **Ln**-Cu catalysts through contact angle measurements. As shown in Figure R5, all **Ln**-Cu catalysts are hydrophobic, and the contact angles are in the range of 133°–150°. No correlation of contact angles with CO_2RR performances was found, suggesting that wettability of the catalysts is not a key factor accounting for the observed difference in CO_2RR selectivity.

Figure R5 was added in the revised SI.

In the revised manuscript, we updated on page 9: Contact angle measurements illustrate that the difference in the observed results is not correlated to hydrophobicity of the catalysts (Supplementary Fig. 29).

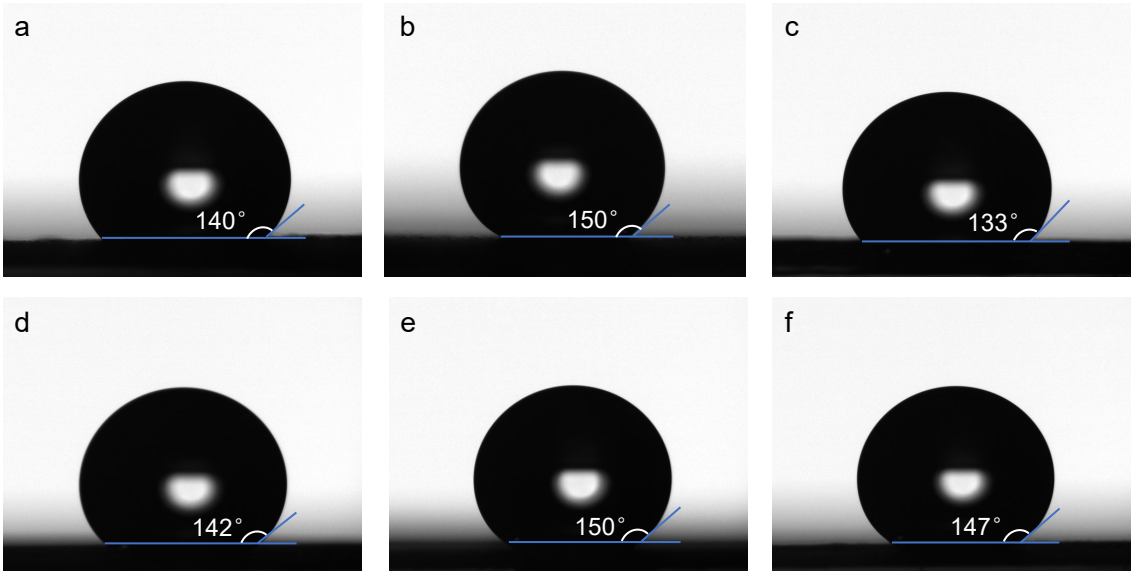

Figure R5 (now added as Supplementary Fig. 29 in SI) | Contact angles of the GDE loaded with Ln-Cu catalysts. a, L1-Cu. b, L2-Cu. c, L3-Cu. d, L4-Cu. e, L5-Cu. f, L6-Cu. The GDE preparation process was detailed in *Methods*. The droplets shown in the figure were 1 M KOH solution.

4. It can be useful to add a sentence in the conclusions to suggest the readers future direction based on the present discovery.

Reply: Inspired by the constructive comments from all three reviewers, we now add the following remark to the Conclusion in the revised manuscript:

Further studies are warranted to synthesise and investigate similar coordination polymers with wider tunability of electronic properties and reaction intermediate adsorption energies, allowing for identifying further structure-function correlations and devising better-performing catalysts.

5. In supplementary Fig.2, it could be beneficial to add the reference pattern of Cu, Cu_2O, CuO and Cu-polymer.

Reply: We have now included the reference XRD patterns of Cu, Cu_2O, CuO and Cu-polymer shown in Figure R6. The XRD patterns of Cu-polymer were simulated from the single-crystal XRD data reported in a previous work (*Journal of Molecular Structure*, 2024, 1305, 137732). The XRD patterns of **L2**-Cu corresponds to the reported Cu-polymer while the broad peak is due to low crystallinity, a common phenomenon of Cu-based polymer crystals (e.g., Figure R7, *Appl. Organometal. Chem.* 2019, 33, e4670).

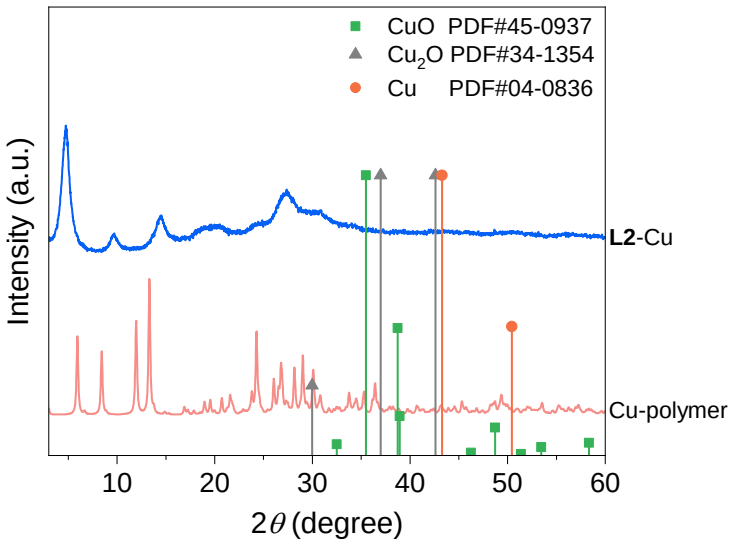

Figure R6 (now added as Supplementary Fig. 3 in SI) | XRD patterns of L2-Cu. The XRD patterns of Cu, Cu_2O, CuO and Cu-polymer were used as references.

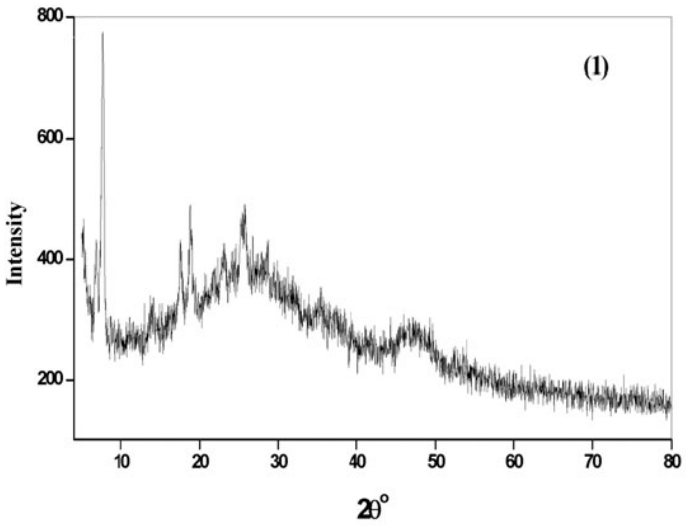

Figure R7 (reproduced from *Appl Organometal Chem.* 2019, 33, e4670) | XRD patterns of a copper polymer. The broad peak was attributed to the low degree of crystallinity.

Reviewer #2:

The authors prepare an interesting array of metal-organic Cu-based ligands for CO2RR and connected a change in CO binding strength and product formation. The Cu tuning and its dynamics are currently of great interest (10.1038/s41467-021-26743-5, 10.1038/s41929-023-01070-8). Due to the huge interest and the importance of a persistent structure in this study to assert the authors claims of rational tuning, it is increasingly important for authors to confirm the in *operando* structure of their material. To assert this, the authors have included a substantial amount of in situ data (e.g. Fig.S13, S15, S17, S20, etc.) However, I have concerns about several

aspects of these in situ studies for stability analysis (laid out below) including: technique limitations, reactor/mass transport-based differences in product formation, and unclear analysis.

Reply: We sincerely thank the reviewer for recognition of the importance of our work. The point-by-point replies are below.

1. A lot of the single-site character and material stability was asserted with XAS e.g. "No metallic Cu–Cu bond was identified, suggesting the single-site nature of formed Ln-Cu (Fig. 2d, Supplementary Fig. 5 and Table 1)." And Figure S13 "No metallic Cu patterns existed after CO2RR, indicating the coordination structure of L2-Cu was maintained" However, previous studies: https://pubs.acs.org/doi/full/10.1021/acscatal.3c01116 have indicated that EXAFS is not sensitive enough to assert the single-site nature of a material. Can the authors comment on this in light of this new understanding of EXAFS limitations?

Reply: Agreeing with the reviewer, we acknowledge the limitation of EXAFS in asserting the single-site nature of materials. Despite this, in light of the feedback from all three reviewers regarding XAS analysis, we have improved the data integrity by re-measuring the XAS spectra of **L2**-Cu post reaction (Figure R8) and re-fitting the *operando* Fourier-transform EXAFS in the range of 0–4 Å (Figure R9 and updated Tables 1 and 6–9 in SI). The results show that the coordination number of Cu keep at ~4. Cu–C bonds only formed under applied potentials and disappeared post reaction.

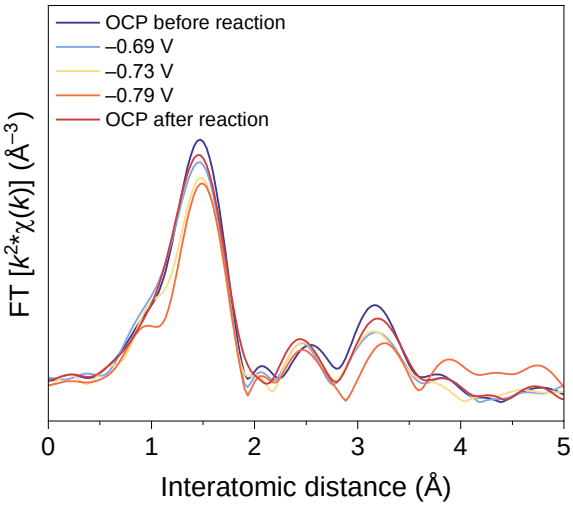

Figure R8 (now added as Supplementary Fig. 25 in SI) | *Operando* Fourier-transform EXAFS spectra for L2-Cu at the Cu *k*-edge.

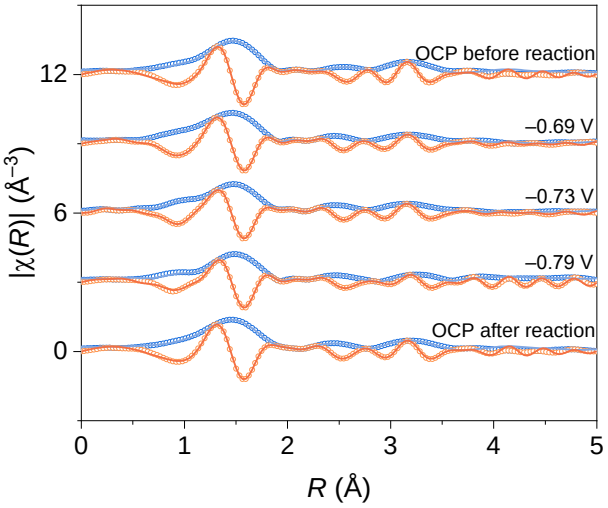

Figure R9 (now added as Supplementary Fig. 26 in SI) | The *operando* Fourier-transform EXAFS spectra (magnitude and imaginary part) for L2-Cu at the Cu *k*-edge, showing the magnitude (experimental data: blue circles; fitting data: blue lines) and imaginary portions (experimental data: orange circles; fitting data: orange lines;) of Fourier transforms of the data. The *k*-range of 2.5–11 $Å^{-1}$ and the *R*-range of 0–4 Å were used for the fits.

In the revised manuscript, we updated on page 8:

Besides, the CN of Cu–O bond recovered to ~2 with the disappearance of Cu–C bond when the applied potential was reversed to open circuit potential (OCP) state (Supplementary Table 9).

To complement the analysis of EXAFS, we have further used *in-situ* IR and Raman spectroscopies for studying the catalyst itself and the interaction between catalyst surfaces and reaction intermediates (*vide infra* for detailed data analyses and discussion), noting that both spectroscopic techniques are surface sensitive.

For *in-situ* IR spectra, we added two spectra measured reversely from high to low overpotentials (updated Fig. 3c in revised MS). The recovered *CO absorption intensity and peak positions indicate the stability of the catalysts.

In the revised manuscript, we updated on page 8:

When reversing the applied potential back to –0.8 and –0.7 V followed by the measurement at –1.1 V, the *CO peak intensities recovered and the *CO peaks blue-shifted to 2,039 and 2,045 cm^{-1}, respectively, the same positions as those in the initial scans.

For *in-situ* Raman spectroscopy, the post-reaction spectra were added to Supplementary Fig. 34, which showed almost the same signals (position and intensity) as those before reaction, indicating stable structure of **Ln**-Cu catalysts.

We also used additional *ex-situ*, bulk analytical tools, including XPS (now added as Figures 19–22 in SI), XRD (updated Figure 16 in SI), SEM (now added as Figure 17 in SI), and SEM-EDS mapping (now added as Figures

5 and 18 in SI) to provide further evidence of the single-site nature and homogeneity of the catalysts, studying the catalysts before and after the CO_2RR measurement.

In the revised manuscript, we updated on page 7:

Additionally, SEM images (Supplementary Fig. 17) in several areas exhibit the well-preserved nanowire morphology. SEM-EDS mapping demonstrates the uniform disperse of Cu after CO_2RR (Supplementary Fig. 18 and Table 15), and XPS spectra of Cu 2*p*, N 1*s*, O 1*s*, and F 1*s* (Supplementary Figs. 19–22) show no change compared to as-prepared **Ln**-Cu. These results collectively suggest that the synthesised coordination polymer catalysts retained their morphologies and chemical properties after CO_2RR.

2. RE: Fig S19: "The weak signals were caused by the interference of ligand molecules existed in the catalysts and lack of localised surface plasmon resonance (LSPR) effect, which is common in metallic Cu-based catalysts" While this does make sense, what is confusing is why you would see in some cases the CO peak go away and come back (e.g. E -0.92 to -1.01) or go away completely (e.g. a, c, d, f). Furthermore, as the authors also note that "COatop species at ~2060 cm-1 was detected on Ln-Cu catalysts, indicating the single-site nature of the catalysts.", it seems like this decrease could be consistent with restructuring. Can the authors comment on this specifically?

Reply: The variations in *in-situ* Raman intensities presented in our original submission were caused by two reasons: (a) the data were collected at varied times using different models of objectives; and (b) the presence of gas bubbles on some occasions during testing forced us to relocate the objective lens to another viewing area of electrode, which did not necessarily have the same local population of active sites. These adverse factors forced us to focus only on analysis of Raman shift information rather than taking into account of the intensities.

In this revised work, we sought clearer understanding of the adsorption behaviours of reaction intermediates, re-measuring the *in-situ* Raman spectra using the same water immersion objective and presenting data where we were able to focus on the same area of view. As illustrated in Figure R10, for all the **Ln**-Cu catalysts, the intensity of *CO peak showed the same trend: increasing initially and then decreasing along with applied potentials. The decrease was attributed by prior reports (e.g., *Nat. Energy* 2020, 5, 478–486) to more consumption of *CO at more negative potentials.

In the revised manuscript, we updated on page 11: The intensity of *CO peaks initially increased followed by a slight decrease, which prior report (*Nat. Energy* 2020, 5, 478–486) ascribed to the rapid consumption of *CO intermediates under more negative potentials.

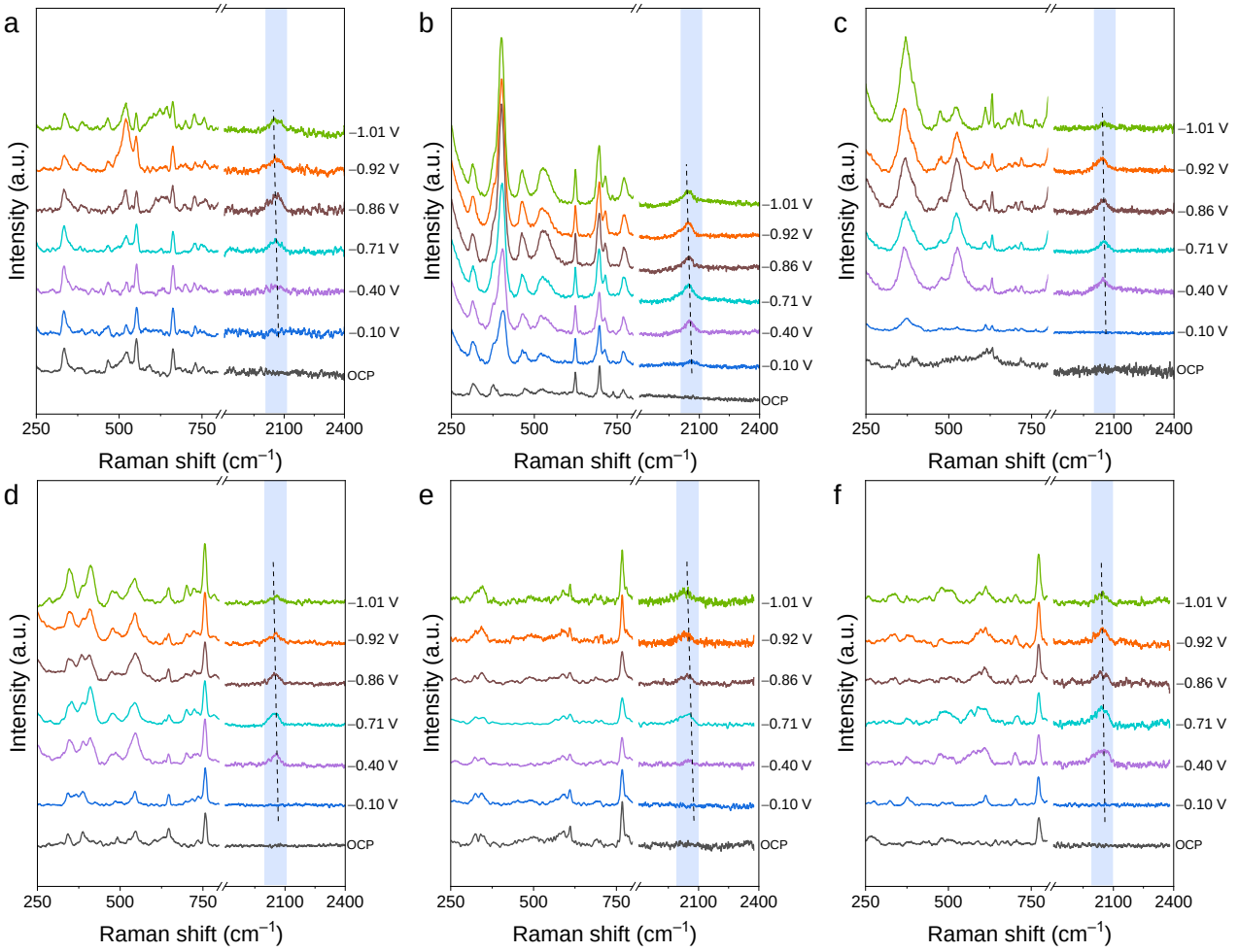

Figure R10 (now added as Supplementary Fig. 32 in SI) | *In-situ* Raman spectra of Ln-Cu during CO_2RR. a, L1-Cu. b, L2-Cu. c, L3-Cu. d, L4-Cu. e, L5-Cu. f, L6-Cu. The *in-situ* Raman spectroscopy was conducted in a flow cell using 0.5 M KOH as the electrolyte with CO_2 flow rate of 5 sccm. Only *CO_{atop} species at ~2,050 cm^{-1} was detected on **Ln**-Cu catalysts, indicating the single-site nature of the catalysts. The *CO peak intensity increased initially and then decreased, attributed to the consumption of *CO at high applied potentials. The weak signals were caused by the interference of ligand molecules existed in the catalysts and lack of localised surface plasmon resonance (LSPR) effect, which is common in metallic Cu-based catalysts.

Similarly, the decrease in *CO adsorption intensity in the *in-situ* IR spectra under high applied potentials is a common phenomenon observed in many studies (e.g., *Nat. Commun*. 2022, 13, 5122), attributed to the rapid consumption of *CO intermediates.

To probe whether the decrease in intensity is caused by restructuring of the **Ln**-Cu catalyst, we reversed the applied potential back to –0.8 and –0.7 V followed by the measurement at –1.1 V. As depicted in Figure R11, the *CO peak intensities recovered and were comparable to those tested from high potential to low potential. This observation further supports the stability of the **Ln**-Cu catalysts and restructuring of the catalyst is unlikely.

In the revised manuscript, we updated on page 8: When reversing the applied potential back to –0.8 V and –0.7 V followed by the measurement at –1.1 V, the *CO peak intensities recovered and the *CO peaks blue-shifted to 2,039 and 2,045 cm^{-1}, respectively, the same positions as those in the initial scans.

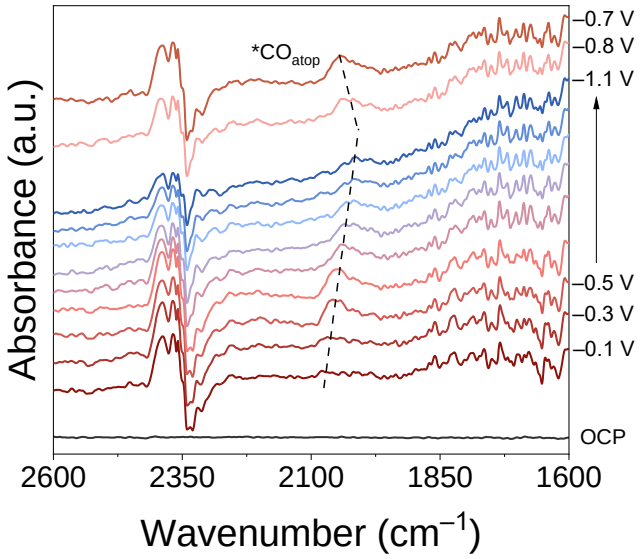

Figure R11 (now updated as Fig. 3c in MS) | *In-situ* FTIR spectra of L2-Cu in CO_2-saturated 0.1 M $KHCO_3$ solution. The *CO_{atop} peaks red-shifted from 2,060 cm^{-1} at −0.3 V to 2,014 cm^{-1} at −1.1 V. When reversing the applied potential back to –0.8 V and –0.7 V, the intensities of *CO recovered and the peaks shifted to 2,039 and 2,045 cm^{-1}, respectively.

3. "The resulting Ln-Cu had similar crystal packing (X-ray diffraction (XRD), Fig. S2)" It is nice that they are similar, however the authors should comment on: 1) the structure, what each peak corresponds to (hkl), 2) why the FWMs are different, esp. peak ~ 28deg 2th. Also, a peak at 5deg 2th is very, very low, what does this structurally represent? Also, XRD was not discussed in the methods. Please give details about the characterization, including the source.

Reply: Our attempt for single crystal X-ray diffraction analysis was compromised by the poor crystallinity quality of the formed coordination polymers. The low degree of crystallinity is attributed to (a) rapid coordination process, which leads to the formation of numerous crystal nuclei, and (b) the presence of flexible ligands and bridged –OH groups. The low crystallinity and small size of crystallite result in large FWHM.

To gain insight into crystal structure of the catalyst, we now provided the refined powder X-ray diffraction (PXRD) data employing GSAS (Figure R12). Furthermore, we listed some possible Miller indices according to simulated crystal structures. For instance, the (0 0 1) peak at 4.75 degrees corresponds to an interplanar spacing of 18.64 Å, which might be attributed to the distance between two interval perpendicular layers as

illustrated in Fig. 2e in the manuscript. The slight difference of (0 0 1) peaks observed amongst **Ln**-Cu samples is caused by the size variation of ligands induced by various substituents.

In the revised manuscript, we updated on page 7: Based on the simulated structure, the calculated refinement matches well with the measured XRD patterns (Supplementary Fig. 12).

We have updated details in PXRD measurement in *Methods* (page 18 in MS): For XRD measurement, each powder sample was loaded into the 0.2 mm deep cavity of a glass sample holder. XRD data from the spinning samples were collected in Bragg-Brentano geometry on a Rigaku Smartlab SE powder diffractometer equipped with a Cu K_α X-ray source ($K_{\alpha1}$ = 1.540598 Å, $K_{\alpha2}$ = 1.544426 Å) operating at 40 kV and 40 mA, a 10 mm length-limiting slit and ½° divergence slits. Diffraction data were collected using an XSPA-400 ER two-dimensional detector.

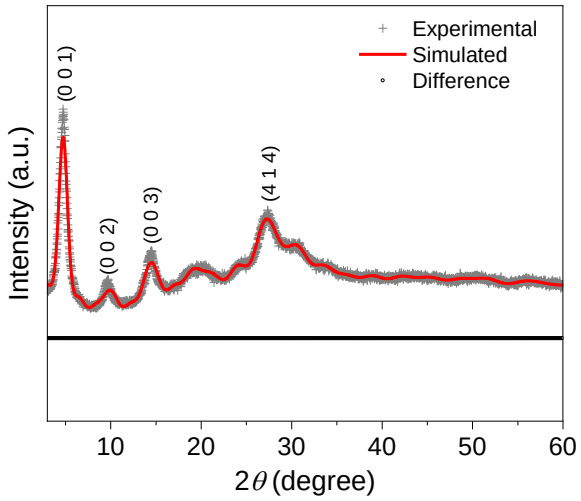

Figure R12 (now added as Supplementary Fig. 12 in SI) | Experimental (grey +) and simulated (red line) PXRD patterns of L2-Cu. The calculated refinement is based on the structure simulated by DFT calculations. The black circle indicates the differences between the experimental data and the refinement. The weighted-profile R factor R_{wp} = 7.41% and χ^2 = 2.06.

4. The authors state for Fig. S13 that "No metallic Cu patterns existed after CO2RR, indicating the coordination structure of L2-Cu was maintained" However, after CO2RR, none of the features present before catalysis seem to remain e.g. major loss of peak at 10, 15, 28, 32. This seems to indicate huge structural changes. Can the authors comment?

Reply: The prominent XRD signals of carbon paper substrate makes it difficult to identify patterns of **L2**-Cu. To address this challenge, we increased the loading amount of **L2**-Cu on carbon paper to 5 mg cm^{-2}. The XRD of **L2**-Cu after reaction were measured after a galvanostatic test at –500 mA cm^{-2} for 1 hour. Although distinct

identification of peaks at 20–30 deg were still hindered by the strong signals from carbon paper, the characteristic peaks of **L2**-Cu at about 5, 10, 15 deg can been clearly observed (Figure R13). Combined with evidence from complementary characterisation such as XPS, SEM and XAS that we elaborated on in response to Q1, we are convinced that the coordination structure of **L2**-Cu was maintained.

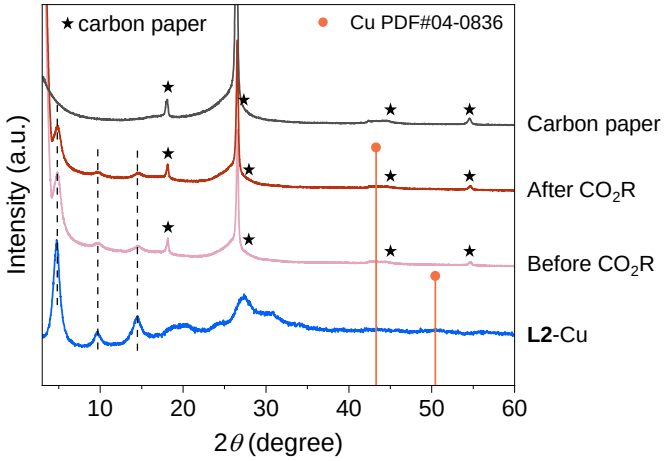

Figure R13 (now added as Supplementary Fig. 16 in SI) | XRD patterns of L2-Cu before and after a long-term CO_2RR performance test. **L2**-Cu was spray-coated on the carbon paper. The signals for carbon paper were listed by star symbols. The XRD patterns of **L2**-Cu after CO_2RR were collected after a galvanostatic test at –500 mA cm^{-2} for 1 hour. The specific patterns of **L2**-Cu located at about 5, 10, 15 degrees were maintained, and no metallic Cu patterns existed after CO_2RR, indicating the **L2**-Cu was not reduced to metallic copper.

5. It has been shown that the cell geometry in CO2RR (10.1016/j.electacta.2022.141698, 10.1016/j.joule.2023.05.010) can impact selectivity dramatically. Can the authors confirm that they have similar selectivity in their different in situ cells? If not, can they discuss / explain what that might mean for their interpretations? Also, please note I have typically seen in situ being used to refer to cells that are in aqueous conditions, with applied potential, but do not confirm product formation, while *operando* measurements confirm product formation. The authors seem to go back and forth (*operando* XAS, in situ IR/RAMAN) without clarifying.

Reply: We agree with the reviewer on terminology of *in-situ* and *operando* and have cited these two references where appropriate to acknowledge the importance of cell geometry in CO_2RR studies in our work. The cell used in our *in-situ* IR studies is similar to the typical H-cell used in many CO_2RR studies (e.g., *Nat. Commun.* 2023, 14, 474). CO_2 mass transport limitation in H-cell would result in difference in CO_2RR product selectivity compared to flow cells. We therefore term the IR as *in-situ* studies with potentials applied and without product quantification, focusing on studying the single-site nature of the catalysts instead of quantifying the adsorption of *CO intermediates of catalyst surfaces.

The *operando* XAS experiments were conducted using a home-made flow cell (Figure R14a, b). Its configuration is same as the flow cell used to evaluate CO_2RR performance, except that Kapton tape was used to seal the gas chamber to allow for X-ray irradiation in and fluorescent signal out. Since analysing gas products at synchrotron radiation site is not practical, we instead evaluated CO_2RR performance in our lab using the same *operando* XAS flow cell and at the same experimental conditions. The performance showed the similar FE of gas products compared to those in a normal flow cell (Figure R14c). We therefore term the XAS as *operando* studies.

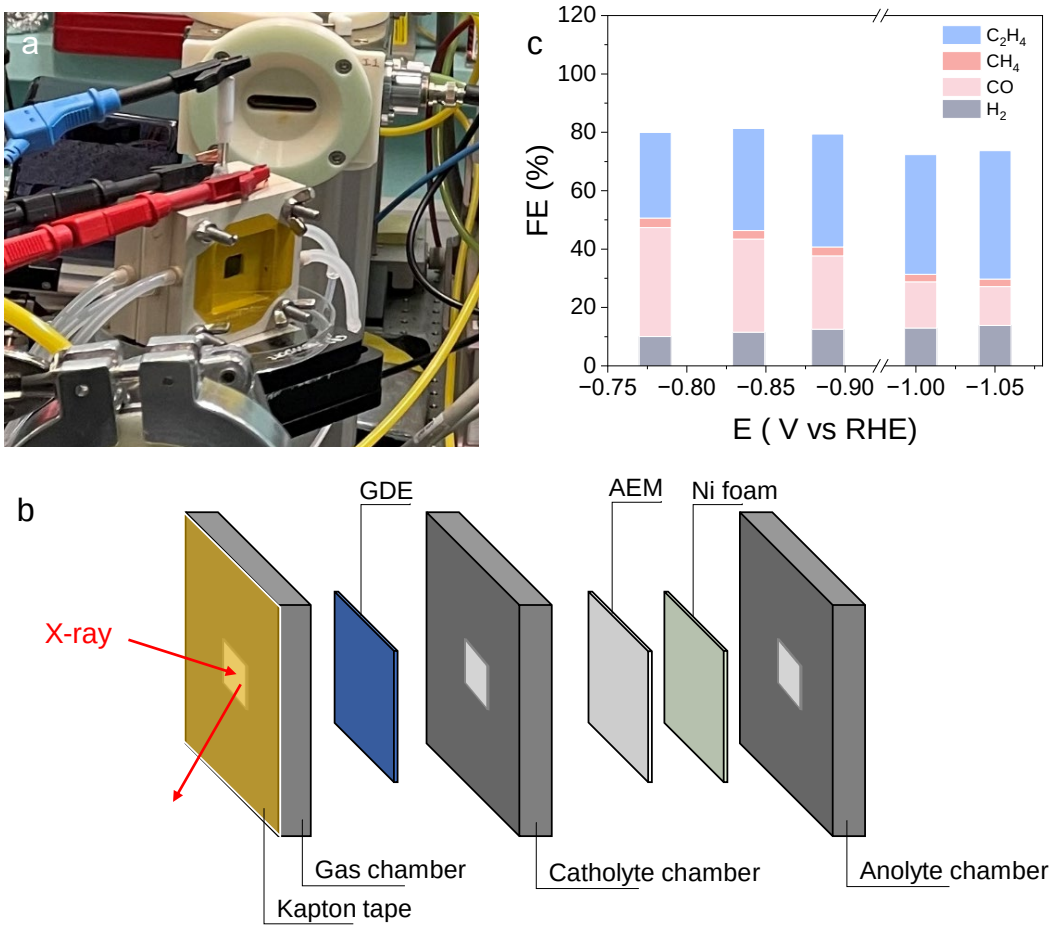

Figure R14 (now added as Supplementary Fig. 24 in SI) | The cell configuration of XAS cell and CO_2RR performance during *operando* XAS test. a, The photograph of *operando* XAFS experiments in operation. **b,** The detailed schematic of the XAS flow cell. **c,** The CO_2RR performance of **L2**-Cu performed in the XAS flow cell.

In-situ Raman cell (schematic shown in Figure R15) is modified and home-made based on the flow cell. To allow the objective to reach the catalyst surfaces, the reference and counter electrodes of the cell are configured to different positions from those in the flow cell for performance test. Such configuration prevents us from measuring CO_2RR product easily and accurately. Thus, we term our Raman spectroscopy as *in-situ* studies.

In the revised manuscript, we have now clearly differentiated the *in-situ* and *operando* studies by stating the experimental conditions and noting whether product analysis was conducted.

On page 18: CO_2RR products were not analysed during *in-situ* Raman test.

On page 19: CO_2RR products were not analysed during *in-situ* IR test.

On page 19: Similar CO_2RR product distribution and selectivity were obtained using the *operando* XAS cell, compared to those using the flow cell for CO_2RR performance test.

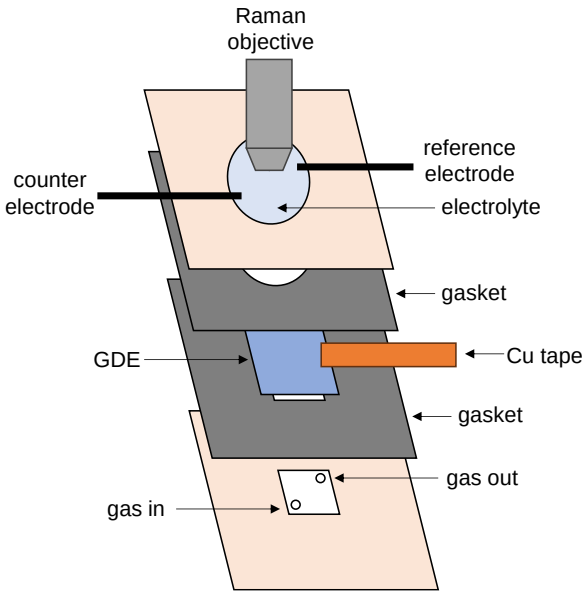

Figure R15 (now added as Supplementary Fig. 31 in SI) | Schematic illustration of the electrochemical cell for *in-situ* Raman measurements. A water immersion objective (Olympus x60 water immersion lens (NA 1.0, WD 2.0 mm)) and a 785 nm laser were used. An Ag/AgCl (saturated KCl) electrode and a Pt wire were used as the reference and counter electrodes, respectively.

6. "Besides, the Raman shifts from 200 cm−1 to 1700 cm−1, typical vibrational modes of Ln-Cu coordination polymers, showed almost no change compared to the spectrum at OCP (Supplementary Fig. 20), which provided complementary evidence of Ln-Cu stability." This does not seem consistent with my interpretation of the figures, especially between 200 and 500 for B, C, E and F. Furthermore, the authors also say "The peaks at 200–1700 cm- 1 correspond to the vibrational modes of molecular structures in Ln-Cu.", but offer no insights into which peak correlated with what within the structure. It would be necessary to have more annotations and analysis of such complex data.

Reply: To clearly correlate each Raman shift peak with the catalyst's structure, we conducted *ex-situ* Raman spectroscopic measurements of the **Ln**-Cu catalysts (Figure R16). The peak assignments of **Ln**-Cu in the range of 250–1,650 cm^{-1} were tabulated as well.

In the revised manuscript, we updated on page 12: Besides, the Raman peaks from 250 cm^{-1} to 1,650 cm^{-1}, positions for typical vibrational modes of **Ln**-Cu coordination polymers, have been assigned in Supplementary Fig. 33.

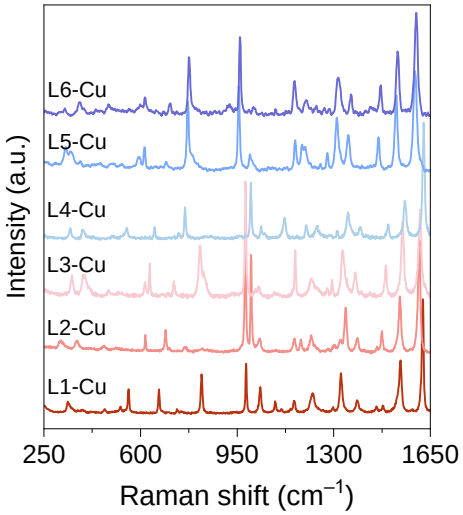

Observed frequency (cm^{-1})	Vibrational assignments
1610 vs	[νCC + δHCC] in benzene
1538 s	νC_bC_t + νNC in triazole + νCC in benzene
1474 w	δHCN + δHCC
1456 vw	νNC in triazole
1385 w	νNC in triazole + δHCN
1342 m	δHCC + δHCN
1218 m	νCC in benzene + νCC in triazole
1181 w	νCC in triazole
1158 w	δHCC
1031 w	νNN in triazole
1000 vs	[νCC + νHCC] in benzene
980 vs	νNC in triazole
691 m	τHCCC
617 m	δCCC
370 w	τbenzene
310 w	δCCC + δCCN

Figure R16 (now added as Supplementary Fig. 33 in SI) | *Ex-situ* Raman spectra of Ln-Cu and peak assignment. The peak assignment is listed based on **L2**-Cu. It is worth noting that the corresponding peaks in other **Ln**-Cu materials may exhibit slight shifts due to the presence of different substituents. Additionally, these substituents may generate corresponding vibrations, such as aromatic νCF (556 cm^{-1}) in **L1**-Cu and νCF (616 cm^{-1}) in **L3**-Cu, aromatic νCCl (761 cm^{-1}) in **L4**-Cu, and νC–OCH3 (1,158 cm^{-1}) in **L6**-Cu. Abbreviations in the table: vs, very strong; s, strong; m, medium; w, weak; vw, very weak; ν, stretching; δ, in-plane bending; τ, torsion.

Re-measurement of *in-situ* Ramans spectroscopy also allowed us to analyse the intensity of Raman peaks in the range of 250–1,650 cm^{-1}. As shown in Figure R17, peak intensity increased and peak position shifted with increase in applied potentials. We attribute these changes to the influence of the electric field. To validate this explanation, we performed an additional test at the OCP after test with applied potentials for each catalyst. It was demonstrated that the Raman peaks recovered to their original states (density and Raman shift). This reversibility also indicated the structural stability of the **Ln**-Cu catalysts.

In the revised manuscript, we updated on page 12: The spectra at OCP state after reaction showed almost no change compared to the spectra at OCP state before CO_2RR (Supplementary Fig. 34), which provided complementary evidence for the stability of **Ln**-Cu.

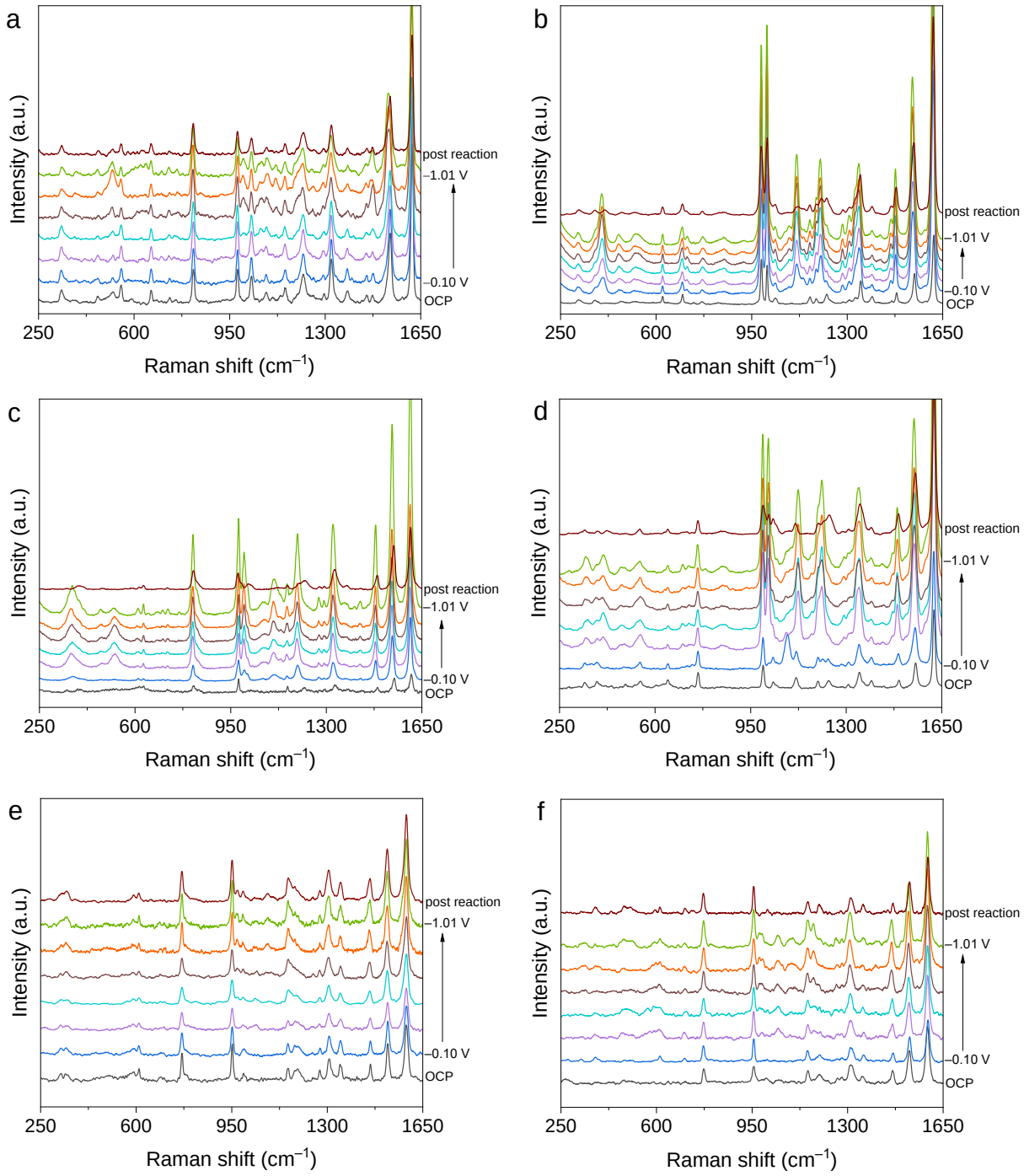

Figure R17 (now added as Supplementary Fig. 34 in SI) | *In-situ* Raman spectra of Ln-Cu during CO_2RR. a, L1-Cu. b, L2-Cu. c, L3-Cu. d, L4-Cu. e, L5-Cu. f, L6-Cu. The peaks at 250–1,650 cm^{-1} correspond to the vibrational modes of molecular structures in **Ln**-Cu. The spectra post reaction showed almost the same signals as those in the spectrum at OCP state before reaction, indicating a stable structure of **Ln**-Cu catalyst. The peaks at ~520 cm^{-1}, ~1,010 cm^{-1} and ~1,060 cm^{-1} are ascribed to Cu–OH, HCO_3^- and CO_3^{2-} (*J. Am. Chem. Soc.* 2020, 142, 15438-15444; *Curr. Opin. Green Sustainable Chem.* 2022, 34, 100589).

7. RE: Fig S8, is F also seen in L1 and L3 Ln-Cu catalysts? Furthermore, is this still seen after catalysis?

Reply: F was observed in **L1**-Cu and **L3**-Cu in XPS spectra (Figure R18). We also measured the F 1*s* XPS spectra of **L1**-Cu and **L3**-Cu after electrolysis. To avoid the interference of F in Nafion solution that we used as a binder, the catalysts were coated on the carbon paper without Nafion. As shown in Figure R18, the F substituents in **L1** and **L3** showed similar XPS peaks before and after electrolysis.

In the revised manuscript, we updated on page 7: XPS spectra of Cu 2*p*, N 1*s*, O 1*s*, and F 1*s* (Supplementary Figs. 19–22) show no change compared to as-prepared **Ln**-Cu.

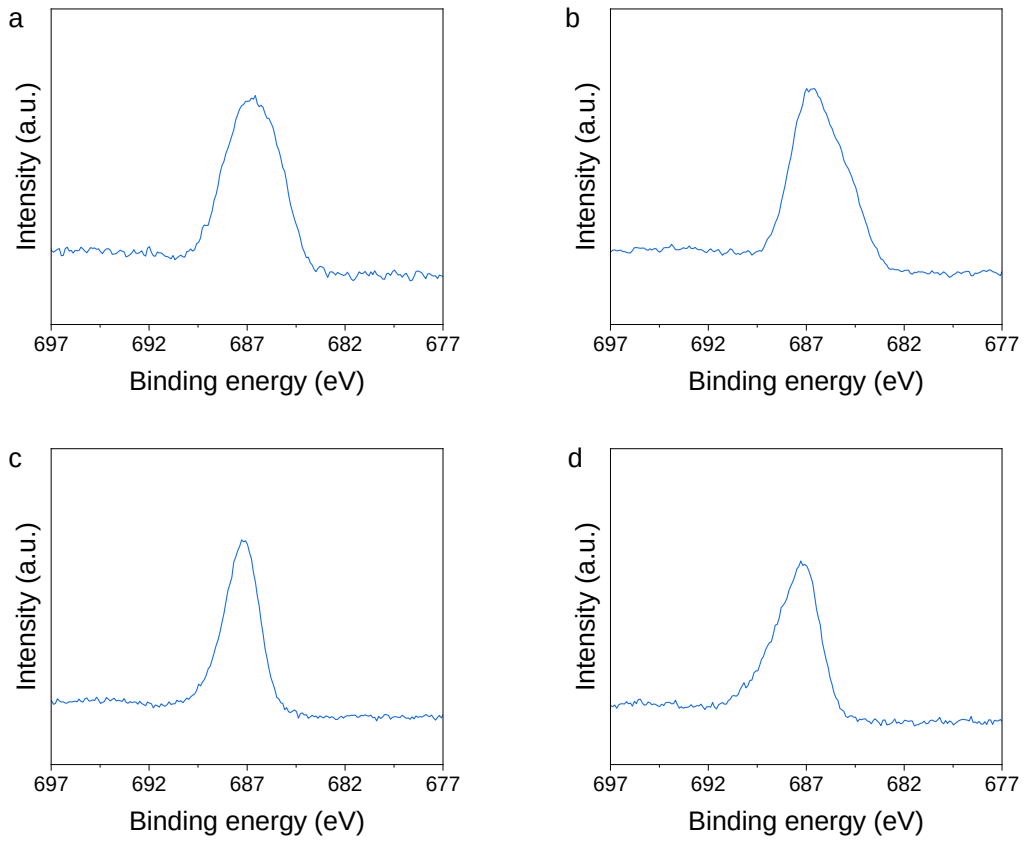

Figure R18 (now added as Supplementary Fig. 22 in SI) | F 1*s* XPS spectra of Ln-Cu before and after electrolysis. a, L1-Cu before CO_2RR. b, L1-Cu after CO_2RR. c, L3-Cu before CO_2RR. d, L3-Cu after CO_2RR. The catalysts were coated on carbon paper without Nafion solution to avoid the interference of F from Nafion.

8. "The Raman spectra of C≡O stretch in the range of 1900–2200 cm−1 showed a redshift from L1-Cu to L6-Cu, under the same applied potential (Fig. 5e)." Do you also see a shift in the raman peak with applied potentials? I think it would be valuable to do the same analysis for Fig S19 and discuss.

Reply: As depicted in Figure R19, in our new Raman spectroscopic data, we did observe a red shift of the C≡O stretching peak in each **Ln**-Cu catalyst with increasing applied potentials. This phenomenon is also found in *in-situ* IR spectra, which can be attributed to the Stark effect of adsorbed species.

In the revised manuscript, we updated on page 11: For each **Ln**-Cu catalyst, the C≡O stretch in the range of 1,900–2,200 cm^{-1} also showed the Stark effect, shifting to lower wavenumbers with applied potentials from –0.10 V to –1.01 V.

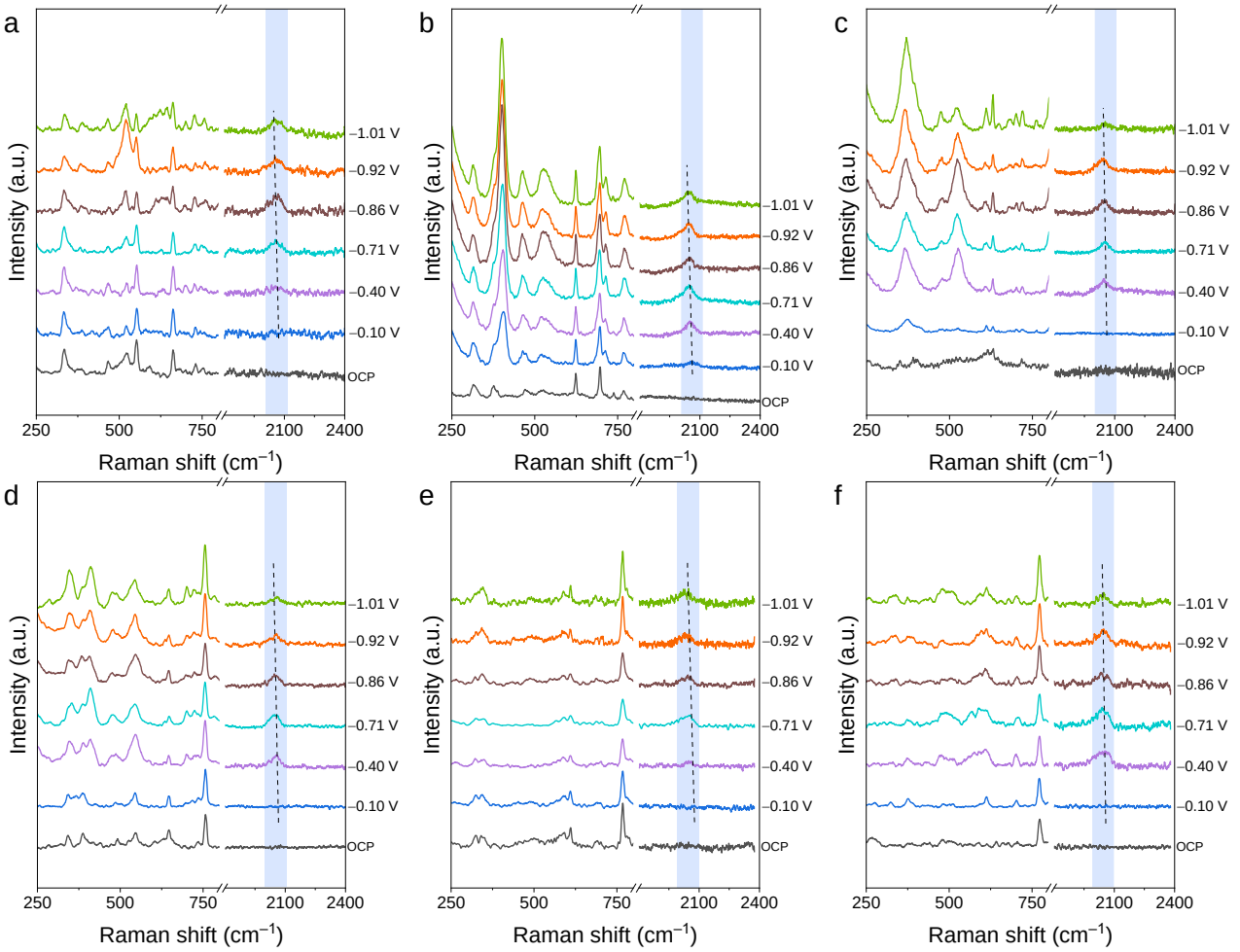

Figure R19 (now added as Supplementary Fig. 32 in SI) | *In-situ* Raman spectra of Ln-Cu during CO_2RR. a, L1-Cu. b, L2-Cu. c, L3-Cu. d, L4-Cu. e, L5-Cu. f, L6-Cu. The *in-situ* Raman spectroscopy was conducted in a flow cell using 0.5 M KOH as the electrolyte with CO_2 flow rate of 5 sccm. Only $*CO_{atop}$ species at ~2,050 cm^{-1} was detected on **Ln**-Cu catalysts, indicating the single-site nature of the catalysts. The *CO peak intensity increased initially and then decreased, attributed to the consumption of *CO at high applied potentials. The weak signals were caused by the interference of ligand molecules existed in the catalysts and lack of localised surface plasmon resonance (LSPR) effect, which is common in metallic Cu-based catalysts.

Reviewer #3 (Remarks to the Author):

The authors report on a system of catalysts composed of Cu in PhTA linear/cross-linked coordination network with varying functionality; electron acceptance/donation from functional groups towards Cu is regulated via the conjugated structure of the linkers. Cu2+ sites are coordinated in plane square geometry by 4 ligands: two network linkers into linear chains, and two substitutable electron donors (**OH-, **Cl-) that cross-link the linear chains. CO2RR electrocatalysis is proposed to take place through replacement of the electron donor groups by *(CO)*(CO), proposed via DFT as precursor to C-C coupling. The authors present in detail the synthesis, electrochemical testing and thorough characterization by many analytical methods and DFT. The central finding is a formulated descriptor eta_{C-C coupling}, describing the efficiency of C-C-coupling as a function of linker functionality and applied potential. Several linear relationships (including a "volcano" plot) are reported between the HOMO level, Bader charge, *CO intermediate bonding at the Cu sites, and eta_{C-C coupling}. The overall quality of the experiments and conclusions is satisfactory, and has the potential of valuable insights into CO2RR catalysis, especially given the large amount of data presented as evidence. However, the data documentation and treatment must be improved as to not cause false interpretation. I cannot evaluate the novelty in the application of the PhTA-Cu system for CO2RR due to my limited expertise in this field, but if considered novel enough by fellow reviewers from the electrochemistry community, I recommend acceptance after major revision.

Reply: We thank the reviewer for their thoughtful observations and recommendation. We have improved the quality of our manuscript and responded the reviewer's comments below, point-by-point.

General remarks: For such a broad-audience journal, reading the paper should be easy and contain sufficient literature references for non-experts. The authors should lead the reader though the many results to concise conclusions. On page 10, after data is presented and the authors arrive at some conclusions, they suddenly start presenting even more data on the Ln-Cu series to derive further conclusions, so I do not know then the paper will finish. I suggest to re-structure the paper and separate it into 4 blocks (in order that the authors find appropriate): synthesis; all non-*operando* characterization of the Ln-Cu series; testing; *operando* studies.

Reply: In light of the reviewer's suggestion, we have now improved the logic flow and readability of the manuscript by structuring the main text into five sections. The revised manuscript now flows:

1. Tuneable Cu electronic states by ligand coordination: We initiated the evaluation of the ligand-tuning method through theoretical calculations.

2. Synthesis and characterization of catalysts: Subsequently, we synthesized the catalysts and characterized their structures.

3. CO_2RR performance and catalyst stability: Using **L2**-Cu as the example catalyst, we elucidated the performance and stability of the catalysts.

4. C–C coupling efficiency: We then extended the evaluation of performance for all **Ln**-Cu catalysts to compare their C–C coupling efficiency, serving a base for mechanistic studies.

5. Mechanism studies: We studies reaction mechanism using various experimental techniques and DFT calculations, establishing the correlation between C–C coupling efficiency and *CO adsorption energy.

Specific remarks:

1. Ln-Cu as a catalyst system can be categorized as a reticular 3D material among other catalyst systems. Please refer to review https://pubs.rsc.org/en/content/articlelanding/2020/CS/D0CS00835D and other work on Cu-based CO2RR-electrocatalysis by B. Roldan Cuenya.

Reply: We acknowledged the similarity between reticular 3D materials and our **Ln**-Cu materials in our initial submission, and thank the reviewer for drawing our attention to Cuenya's work. We have now cited important works by B. R. Cuenya (*Chem. Soc. Rev.*, 2020, 49, 6884–6946; *Nat. Energy*, 2024, DOI: 10.1038/s41560-024-01461-6) in the revised Introduction section to contextualise our studies of coordination polymer catalysts.

2. The authors claim to have derived a "volcano plot" for eta_CCcoupling - the term is known from work by J. Nørskov for describing activity as a function of descriptors. Only 1 point on the left side of the "volcano" (L1-Cu) is insufficient, more points are needed to verify the significance. There are already several linear trends derived in this study, and L1-Cu is an outlier in terms of eta_CCcoupling. I would address this trend as "volcano-like due to outlier", focus on the other linear relationships as central finding, and leave space for future studies. Or work with only L2-L6, and place L1-Cu into Supporting Information.

Reply: We agree with the reviewer that the single point on one side of the volcano plot increases uncertainty of the conclusion. While we are reluctant to go to the opposite direction – a linear correlation, from which one may conclude weaker binding of *CO always leads to better C–C coupling efficiency, we have now added a remark in the Conclusion section to highlight such uncertainty and call for further studies.

In the revised Conclusion, we now write: Further studies are warranted to synthesize and investigate similar coordination polymers with wider tunability of electronic properties and reaction intermediate adsorption energies, allowing for further structure-function correlations and devising better-performing catalysts.

3. Why do the authors call C2 products C2+? Do they believe that C3 and higher can be produced via the proposed reaction mechanism, analogous to Fischer-Tropsch synthesis? If yes, please explain. If no, call the products C2.

Reply: We have revised all C_{2+} to C_2 throughout the main text and Supplementary Information.

4. The authors propose *CO to be the key intermediate for C2+ selectivity. Please provide sufficient evidence from literature, including the one mentioned above, for what intermediate is key for CO2RR. E.g. the paper https://pubs.acs.org/doi/10.1021/acs.jpcc.0c10736 assumes *CO as part of the mechanism, but traditionally, non-CO2-based cross-coupling knows many other mechanisms and reactants (see e.g. https://en.wikipedia.org/wiki/Cross-coupling_reaction).

Reply: We have cited prior reports that proposed *CO as the key intermediate (*J. Phys. Chem. C* 2021, 125, 4, 2464–2476; *ACS Catal.* 2020, 10, 1754−1768; *Nat Catal.* 2018, 1, 922–934). Consistent with these reports, in our study, only *CO intermediate was observed under CO_2RR operating conditions, suggesting that *CO is involved as a reactant in the rate-determining step. While other cross-coupling reaction mechanism cannot be excluded, we are inclined to believe *CO plays an important role in forming C_2 products.

In the revised manuscript, we updated on page 11: In previous studies (*J. Phys. Chem. C* 2021, 125, 4, 2464–2476; *ACS Catal.* 2020, 10, 1754−1768; *Nat Catal.* 2018, 1, 922–934), the adsorption of *CO intermediate plays a critical role in determining $\eta_{C-C\ coupling}$. We therefore further studied the *CO binding strength on Cu in **Ln**-Cu catalysts.

5. Page 8, Line 17: The HOMO level can be tuned by varying the linker functionality, and this directly correlates towards activity. Can the authors explain this dependency in terms of bonding strength and mechanism?

Reply: In coordination polymers, the coordination bonds are formed by electron transfer from ligand to metal. The principles of bonding—energy similarity, orbital overlap, and symmetry—are crucial to understanding these interactions. In our work, when the ligands coordinating with Cu ions, the energy similarity is a significant factor in determining the strength of these bonds because of the similar orbital overlap and symmetry of all these ligands sharing the common phenyl triazole structures: when the HOMO energy of a ligand is closer to that of the copper orbitals, a stronger coordination bond is formed. Specifically, a higher HOMO level of the phenyl triazole ligand is in better energy alignment with copper orbitals, leading to a more robust electron exchange between Cu and phenyl triazole and thereby a greater reduction in the electron state of Cu^{2+}. *CO bonds with Cu (orbital structure $Cu^{(2-\delta)+}$ ($[Ar]3d^{9+\delta}$) in this work) through its 5σ orbital and π* orbital (i.e., back-donation) and the contribution share of each determines the overall binding strength (*J. Am. Chem. Soc.* 1985, 107, 578-584).

6. The quantity eta_CCcoupling is a function of FE, but it is not explained how FE is determined/calculated. Please explain this; apparently it is not straightforward, refer to literature such as https://pubs.acs.org/doi/10.1021/acsenergylett.3c02362.

Reply: We have added the calculation of FE in the *Methods* part, including the calculation of FE for gas and liquid products.

In the revised manuscript, we updated in the *Methods* (page 17): The FE for a specific product was calculated according to the following equation:

$$FE_{product} = \frac{C_{product} \times V \times N \times F}{Q} \times 100\%$$

$C_{product}$: the measured concentration of the specific product, mole per liter (mol/L, M);

V: the volume of the electrolyte for liquid products and the total gaseous volume for gaseous products, liter (L);

N: the number of electron transfer for the formation of a specific product;

F: Faradaic constant, 96485 C mol^{-1};

Q: total quantity of electric charge, coulomb (C).

Besides, we added the calibration curves for liquid product quantification using NMR to the Supplementary Information (Figure R20).

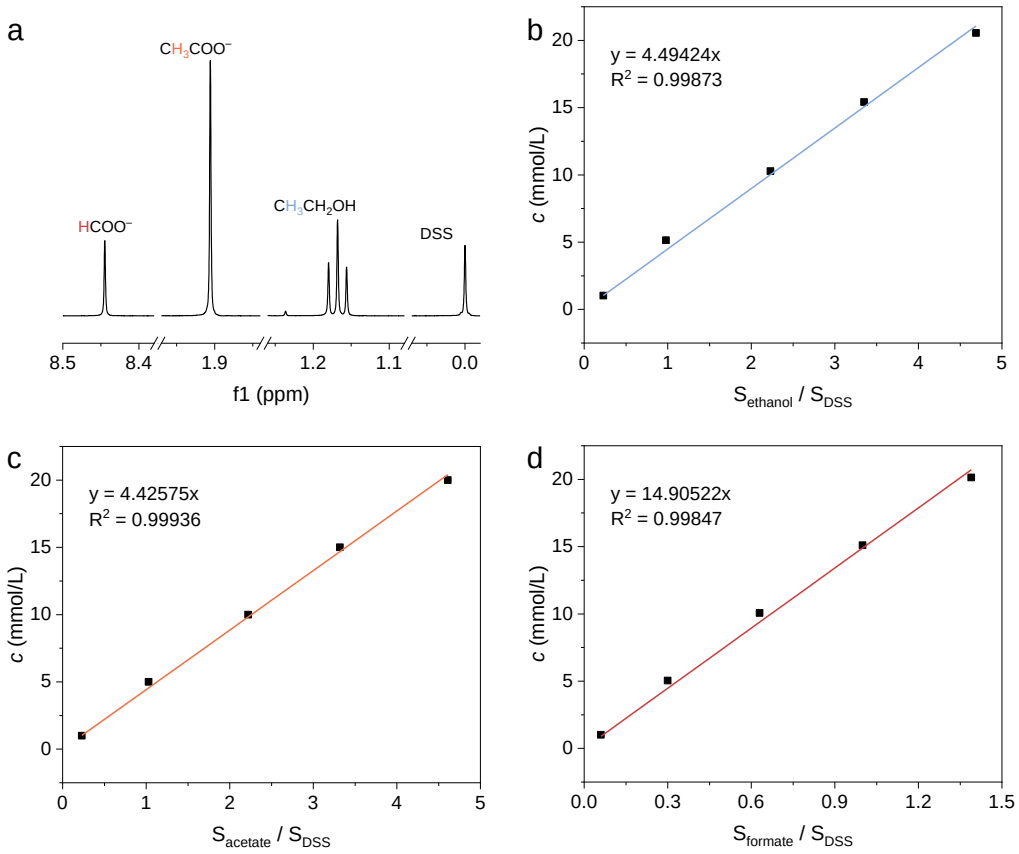

Figure R20 (now added as Supplementary Fig. 37 in SI) | ^{1}H-NMR spectra of liquid products and calibration plots. a, ^{1}H-NMR spectrum for ethanol (1.17 ppm), acetate (1.91 ppm) and formate (8.44 ppm). **b,** Calibration plot for ethanol measured in 1 M KOH electrolyte. **c,** Calibration plot for acetate measured in 1 M KOH electrolyte. **d,** Calibration plot for formate measured in 1 M KOH electrolyte. 6 mmol L^{-1} of 3-trimethylsilyl-1-propane sulfonic acid sodium salt (DSS) was used as an internal standard to quantify the concentration of each liquid product.

7. XRD

7.1 Suppl Fig 2: check axis increments, and make them comparable to other XRD data presented in paper and SupplInfo.

Reply: We have adjusted the axis increments of XRD data and made them consistent (Figure R21).

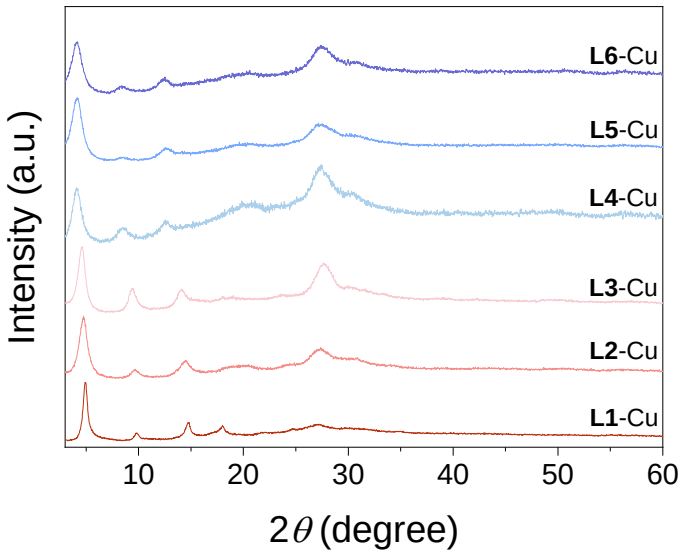

Figure R21 (now added as Supplementary Fig. 2 in SI) | XRD patterns of Ln-Cu.

7.2 The reflections of Ln-Cu are quite broad. Can the authors add reference lines from database or own refinement for Ln-Cu (at least L2-Cu) to indicate where to expect reflections.

Reply: Our attempt for single crystal X-ray diffraction analysis was compromised by the poor crystallinity quality of the formed coordination polymers. The low degree of crystallinity is attributed to (a) rapid coordination process, which leads to the formation of numerous crystal nuclei, and (b) the presence of flexible ligands and bridged –OH groups. The low crystallinity and small size of crystallite result in large FWHM.

To gain insight into crystal structure of the catalyst, we now provided the refined powder X-ray diffraction (PXRD) data employing GSAS (Figure R22). Furthermore, we listed some possible Miller indices according to simulated crystal structures. For instance, the (0 0 1) peak at 4.75 degrees corresponds to an interplanar spacing of 18.64 Å, which might be attributed to the distance between two interval perpendicular layers as illustrated in Fig. 2e in the manuscript. The slight difference of (0 0 1) peaks observed amongst **Ln**-Cu samples is caused by the size variation of ligands induced by various substituents.

In the revised manuscript, we updated in page 7: Based on the simulated structure, the calculated refinement matches well with the measured XRD patterns (Supplementary Fig. 12).

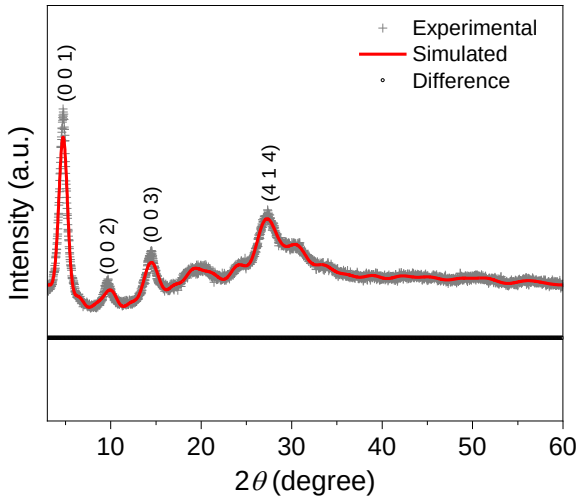

Figure R22 (now added as Supplementary Fig. 12 in SI) | Experimental (grey +) and simulated (red line) PXRD patterns of L2-Cu. The calculated refinement is based on the structure simulated by DFT calculations. The black circle indicates the differences between the experimental data and the refinement. The weighted-profile R factor R_{wp} = 7.41% and χ^2 = 2.06.

7.3 Suppl Fig 13: the authors claim that no metallic Cu seen. What are the small bumps in the C2-Cu pattern at the position where Cu metal reference lines are located? (for this reason, please give reflection position for Ln-Cu).

Reply: We have re-measured the XRD of **L2**-Cu loaded on carbon paper before and after CO_2RR (Figure R23). The small bumps come from the carbon paper which have been labelled in the revised figures.

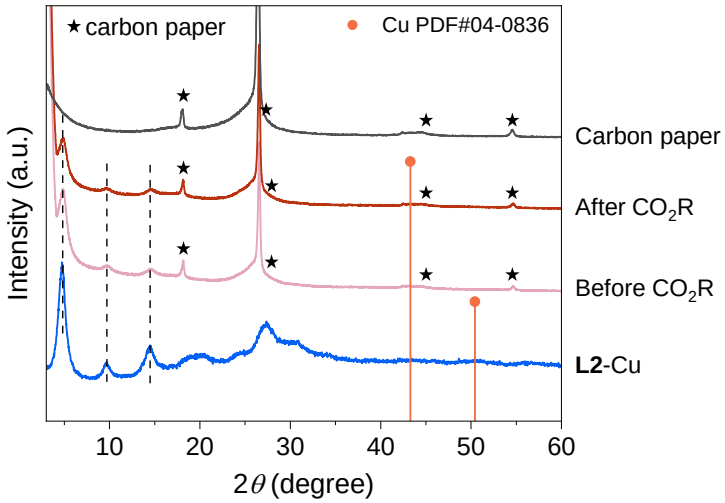

Figure R23 (now added as Supplementary Fig. 16 in SI) | XRD patterns of L2-Cu before and after a long-term CO_2RR performance test. **L2**-Cu was spray-coated on the carbon paper. The signals for carbon paper were labelled by star symbols. The XRD patterns of **L2**-Cu after CO_2RR were collected after a galvanostatic test at –500 mA cm^{-2} for 1 hour. The characteristic patterns of **L2**-Cu located at about 5, 10, 15 degrees were maintained, and no metallic Cu pattern emerged after CO_2RR, indicating the **L2**-Cu was not reduced to crystalline copper.

7.4 Supp Fig 13 and 17: Comparisons are made between pure catalysts prior to testing, and catalysts on carbon paper after testing. The comparison is very inconclusive because of the large difference caused by the carbon paper. Can the authors indicate the important reflections, or compare the catalysts prior to testing also deposited on carbon paper?

Reply: We have re-measured the XRD of **L2**-Cu(Cl) deposited on carbon paper before CO_2RR (Figure R24). Before CO_2RR, only the peak at ~6.6 degree of **L2**-Cu(Cl) can be seen when **L2**-Cu(Cl) was deposited on carbon paper, and other peaks arose from carbon paper. After CO_2RR, the peak at ~6.6 degree disappeared and a new peak at ~4.8 degree emerged, consistent with the transformation of **L2**-Cu(Cl) to **L2**-Cu(OH) after CO_2RR.

We have updated the Figure R25 to the revised Supplementary Information.

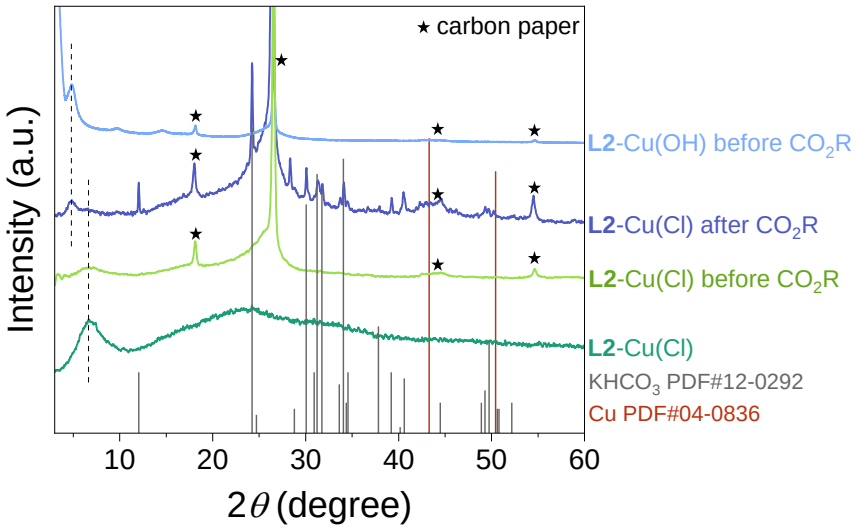

Figure R24 | XRD patterns of L2-Cu(Cl) on carbon paper before and after CO_2RR.

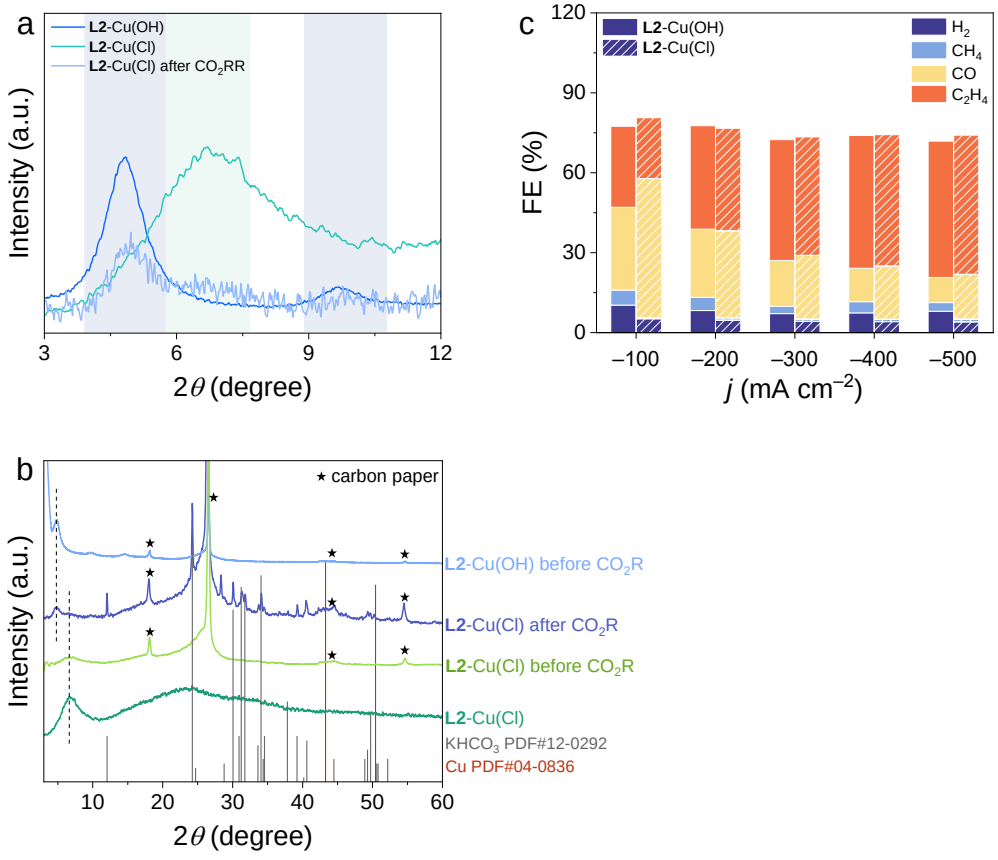

Figure R25 (now added as Supplementary Fig. 28 in SI) | The ligand exchange of L2-Cu exhibited in XRD patterns. a, The transformation from **L2**-Cu(Cl) to **L2**-Cu(OH). **b,** XRD patterns of **L2**-Cu(Cl) on carbon paper before and after CO_2RR. **c,** CO_2RR performance of **L2**-Cu(Cl) in 1 M KOH electrolyte.

8. The TEM images presented are not HR-TEM; please correct this throughout. Please briefly clarify whether only the sample is visible, or TEM grid material (e.g lacey C) is also visible. Please specify the details of TEM sample preparation and acquisition details in Methods.

Reply: We have corrected the term to "TEM". In Figure R26, both the sample and TEM grid material were visible. We deliberately selected clean areas without grids, as depicted in the right picture.

Furthermore, we have provided additional details in the *Methods* section for TEM characterisation: TEM images were acquired using a Talos F200X field-emission transmission electron microscope operating at an accelerating voltage of 200 kV. To prepare the sample for TEM imaging, 0.1 mg of **Ln**-Cu samples were mixed with 0.5 mL of ethanol solution and sonicated for 1 hour. The resulting evenly-dispersed solution was drop-casted onto a Lacey Carbon Supported Mo grid (200 mesh) and dried under infrared light.

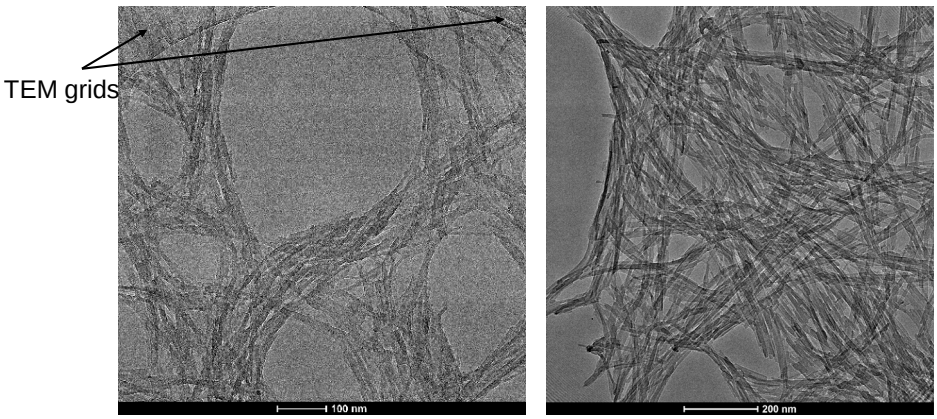

Figure R26 | TEM figures of L2-Cu.

9. FTIR/Raman

9.1 Please check and compare vibrational speciation of the CO peak, and explicitly mention which wavenumbers are relevant. In Fig 3 (c) (FTIR) and 5 (e) (Raman), the CO peak appears very vague. Please adjust the stacking and scaling such that the peak shape and maximum is clearly visible.

Reply: We have rescaled the axis to make the *CO peak more clearly seen (Figure R27). We have also improved clarity of wavenumber ascription.

In the revised manuscript, we wrote on pages 7–8: Using **L2**-Cu as a representative, we only observed atop adsorbed *CO intermediate (*CO_{atop}) formed under applied potentials from –0.3 V to –1.1 V in the *in-situ* IR spectra, with peaks shifting from 2,060 cm^{-1} to 2,014 cm^{-1} (Fig. 3c)…When reversed the applied potential back to –0.8 and –0.7 V followed by the measurement at –1.1 V, the *CO peak intensities recovered and the *CO peaks blue-shifted to 2,039 and 2,045 cm^{-1}, respectively, the same positions as those in the initial scans.

Page 11: The *CO_{atop} stretch shifted from 2,067 cm^{-1} in **L1**-Cu to 2,036 cm^{-1} in **L6**-Cu.

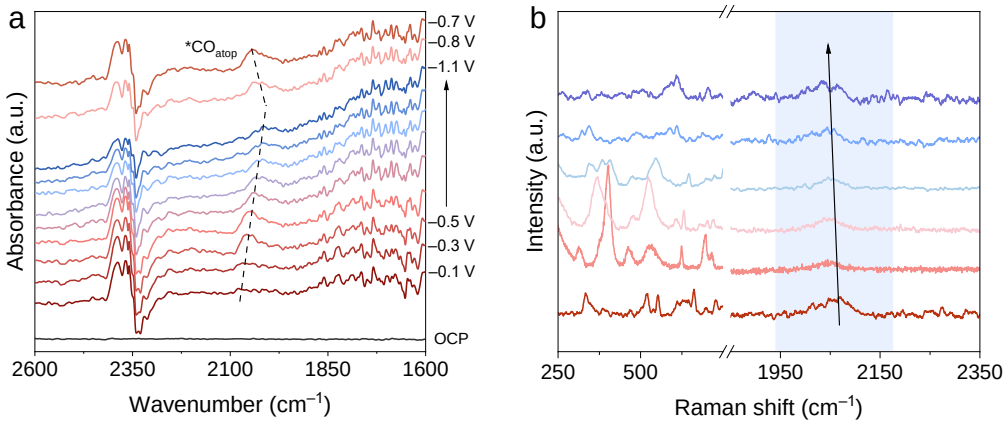

Figure R27 (now updated as Fig. 3c and Fig. 5e in MS) | The rescaled *in-situ* FTIR and Raman spectra. **a**, *In-situ* FTIR spectra of **L2**-Cu catalyst. **b**, *In-situ* Raman spectra of **Ln**-Cu at –0.86 V.

9.2 Fig 5 (d): how are the decay curves "normalized"? An exponential decay cannot go to zero! Please check and correct.

Reply: We have updated the data processing method using an exponential fitting function (Figure R28). In detail, for any given catalyst, all absorption intensities from 0 to 600 seconds were normalised by the initial absorption intensity at $t = 0$. We then used the ExpAssocDecay1 function for curve fitting using OriginPro:

$$y = Yb + A * (1 - \exp(-(x - TD)/Tau))$$

TD (Time offset): x value at which exponential begins;

Yb (Baseline): y value before exponential begins;

A (Amplitude): change in response;

Tau: Time constant

The fitting details have been updated in the *Methods* (page 18 in the revised manuscript):

For any given catalyst, all absorption intensities from 0 to 600 seconds were normalised by the initial absorption intensity at $t = 0$. We then used the ExpAssocDecay1 function for curve fitting using OriginPro:

$$y = Yb + A * (1 - \exp(-(x - TD)/Tau))$$

TD (Time offset): x value at which exponential begins;

Yb (Baseline): y value before exponential begins;

A (Amplitude): change in response;

Tau: Time constant

Besides, we updated the manuscript on page 11: All absorption intensities of the CO desorption process were normalised and fitted by an exponential function (see details in *Methods*) and showed a decreased desorption rate from **L1**-Cu to **L6**-Cu (Fig. 5d), suggesting an increase of CO binding strength from **L1**-Cu to **L6**-Cu.

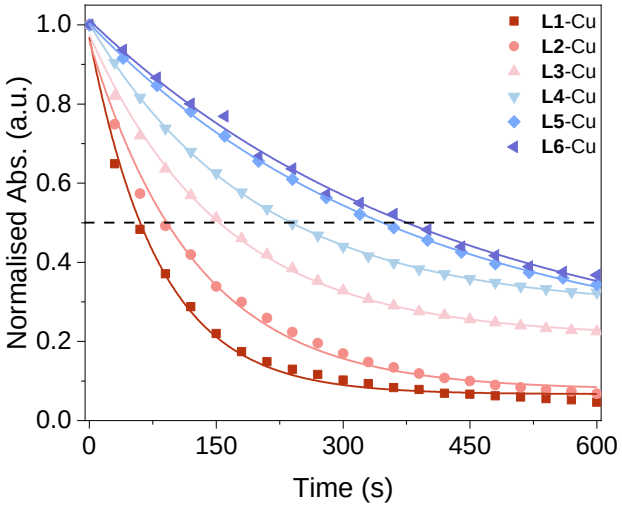

Figure R28 (now updated as Fig 5d in MS) | CO decay curves which shows the desorption rate of adsorbed CO on Cu active sites in different catalysts.

10. XANES

10.1 Fig 3 (d): The authors claim that the XANES spectra remain unchanged during reaction at different potentials and show a stacked plot where no changes are visible. Can the authors show the spectra overlapped to emphasize any minute changes? I would expect some very small variations especially when different potentials are applied, and the intermediate species are in contact with Cu. Also narrow the plot range to e.g. 8970-9030 eV. to show the spectra in better detail.

Reply: We have now overlapped the XANES spectra and narrowed the plot range to 8,970–9,010 eV. Consistent with the reviewer's posit, there are minimal variations under different applied potentials. As shown in Figure R29, the pre-edge peaks and the absorption energy showed that the oxidation states of Cu under all potential ranges are close to +2, with slight decrease under applied potential from –0.69 V to –0.79 V. The result is in line with the FT-EXAFS fitting results: O element has larger electronegativity compared to C element, leading to slight decrease in the Cu oxidation.

In the revised the manuscript (page 8), we wrote that "The XANES spectra showed that the oxidation states of Cu under all applied potentials are close to +2, with slight decrease under applied potential from –0.69 V to –0.79 V (Fig. 3d and Supplementary Fig. 25). FT-EXAFS fitting showed that the slight change of Cu oxidation state originated from the dynamic coordination environment during CO_2RR process…".

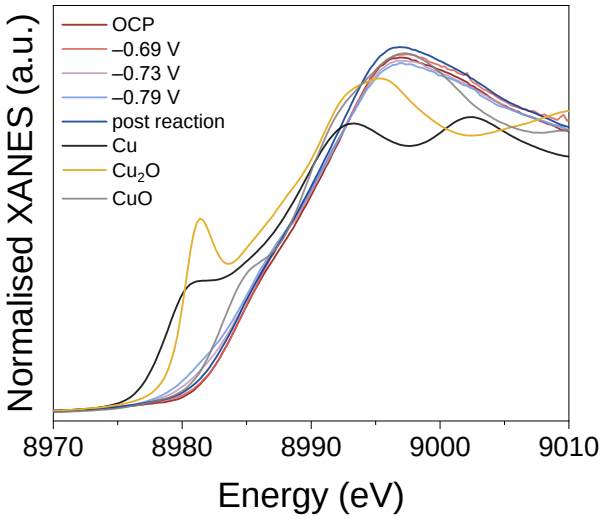

Figure R29 (now updated as Fig. 3d in MS) | *Operando* Cu K-edge XANES of L2-Cu at the applied potentials of −0.69 V to −0.79 V during CO_2RR in a customised flow cell. Reference samples: Cu (black), Cu_2O (yellow), and CuO (grey).

10.2 Page 5, Line 17: Please specify "The *local* atomic structure...".

Reply: We have added "local" to the revised manuscript (Page 6).

10.3 Fig 2 (c): Please show the detail of the Cu K-pre-edge peak, which is characteristic for Cu2+.

Reply: We have added an enlarge region to Fig 2c and designated the Cu K-pre-edge peak in **L2**-Cu catalyst (Figure R30). We also added corresponding description in the revised manuscript (page 6): Besides, the XANES of **L2**-Cu showed the K-pre-edge peak, which is characteristic for Cu^{2+}.

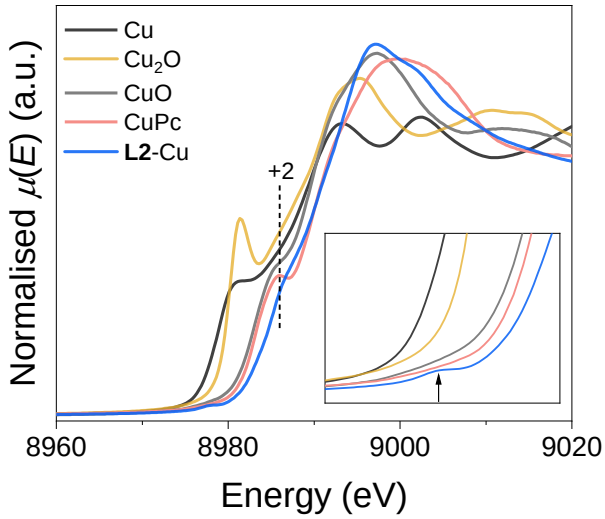

Figure R30 (now updated as Fig. 2c in MS) | Cu K-edge XANES spectrum of L2-Cu. The inset displays a magnification of the pre-edge peak.

11. EXAFS: The presentation and analysis of the EXAFS spectra must be improved significantly, as follows.

Reply: We have actioned each comment as below.

11.1 The EXAFS must be presented as FT-EXAFS (magnitude and imaginary part) in the main text and EXAFS in k-space in SuppInfo. The individual curves must be stacked. If fits are included, they are overlapped with the data. See examples in e.g. https://chemistry-europe.onlinelibrary.wiley.com/doi/full/10.1002/cctc.202200573.

Reply: We have corrected the terms of EXAFS in both main text and SI. The curves have been stacked, and the fitting curves have been overlapped with the experimental data (Figures R31 and R32).

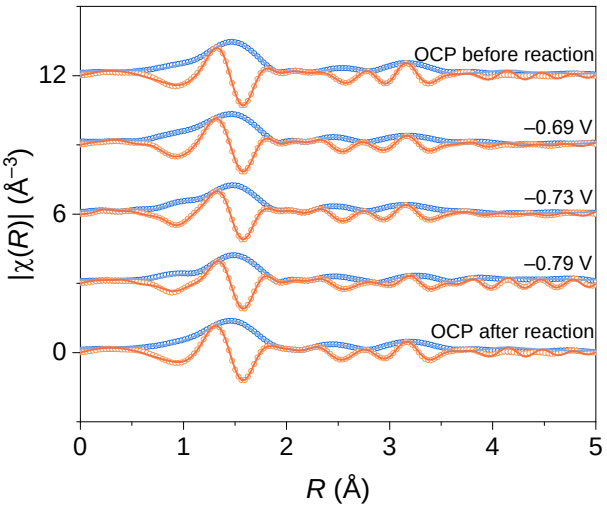

Figure R31 (now added as Supplementary Fig. 26 in SI) | The *operando* Fourier-transform EXAFS spectra (magnitude and imaginary part) for L2-Cu at the Cu *k*-edge, showing the magnitude (experimental data: blue circles; fitting data: blue lines) and imaginary portions (experimental data: orange circles; fitting data: orange lines;) of Fourier transforms of the data. The *k*-range of 2.5–11 $Å^{-1}$ and the *R*-range of 0–4 Å were used for the fits. EXAFS spectra and fits in *k*-space are provided in **Supplementary Fig. 27**. The corresponding fitting results were shown in **Supplementary Tables 1 and 6–9**.

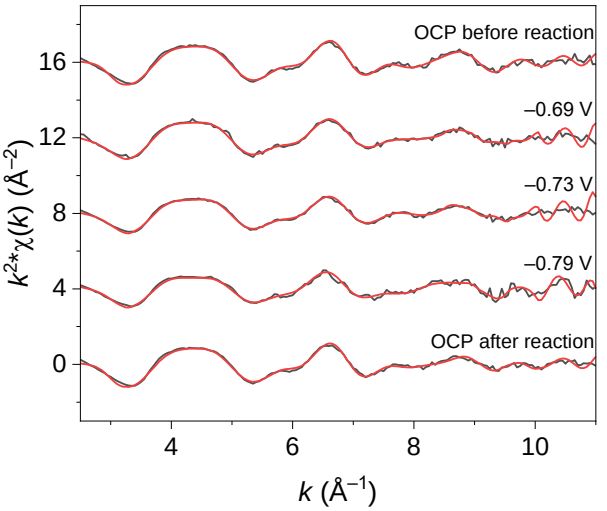

Figure R32 (now added as Supplementary Fig. 27 in SI) | EXAFS spectra and fits in *k*-space at the Cu *k*-edge. Experimental date: dark grey; fitting data: red. Corresponding XANES and Fourier-transform EXAFS are shown in **Fig. 3d** and **Supplementary Fig. 26**.

11.2 What do the authors achieve with wavelet transforms? To my knowledge, WTs are used to estimate whether the peaks in FT-EXAFS originate in light elements (correlate with low k) or heavy elements (correlate with high k) - this, together with any other knowledge gained, must be stated. The k-space and R-space spectra used for the WTs must be shown (e.g. in SupplInfo).

Reply: As the updated FT-EXAFS analyses now provide sufficient information for mechanistic studies, we have now removed the wavelet transforms.

11.3 Please mention the k-range and R-range used for fitting.

Reply: We have added *k*-range and *R*-range used for each fitting:

In the updated manuscript (page 6): Fig. 2d, Cu K-edge FT-EXAFS spectrum and fitting of **L2**-Cu. The *k*-range of 2.5–11 $Å^{-1}$ and the *R*-range of 0–4 Å were used for the fit.

In SI (page 29): **Supplementary Fig. 26 | The *operando* Fourier-transform EXAFS spectra (magnitude and imaginary part) for L2-Cu at the Cu *k*-edge**, showing the magnitude (experimental data: blue circles; fitting data: blue lines) and imaginary portions (experimental data: orange circles; fitting data: orange lines;) of Fourier transforms of the data. The *k*-range of 2.5–11 $Å^{-1}$ and the *R*-range of 0–4 Å were used for the fits. EXAFS spectra and fits in *k*-space are provided in **Supplementary Fig. 27**. The corresponding fitting results were shown in **Supplementary Tables 1 and 6–9**.

11.4 When reporting fit results, also S02, sigma2, deltaE0 and R-factor must be stated in the table.

Reply: We have updated these parameters in Table R4–R8 (added as Tables 1 and 6–9 in the revised SI). The details are shown in our response to Q11.5 below.

11.5 The authors use a very detailed model for fitting the first coordination shell, with C, N and O as back-scatterers, displaced by small shifts from 2 Å. Further shells are neglected. The first problem is that the three neighboring back-scatterers have very similar scattering factors and are therefore usually not distinguishable - the correct/realistic approach would be to use a single shell Cu-O/N/C and refine one distance. If several distances are really possible to resolve, a comparison between a fit with 3 distances and a fit with 1 single distance must be made, where the former has a smaller R-factor or chi^2 than the latter. In that case, a path analysis (plotting the individual shells, preferably as Imaginary part of FT-EXAFS) would be helpful. The second problem is the neglectance of further shells up to 3.5–4.0 Å. Including these shells to the model will significantly justify the use of EXAFS, which is to verify the structure integrity from the point of view of local atomic order.

Reply: We have fitted the data using single Cu–N scatter path and mixed Cu–C/N/O scatter paths (Figure R33) and evaluated the fitting quality correspondingly (Table R3). It is obvious that fitting with Cu–C/N/O scatter paths has much smaller R-factors compared to the single Cu–N scatter path. The data suggested, under applied

potentials, an increase of Cu–C coordination numbers while a decrease of Cu–O coordination numbers. After CO_2RR, **L2**-Cu reversed to its original coordination state, consistent with our mechanistic analyses.

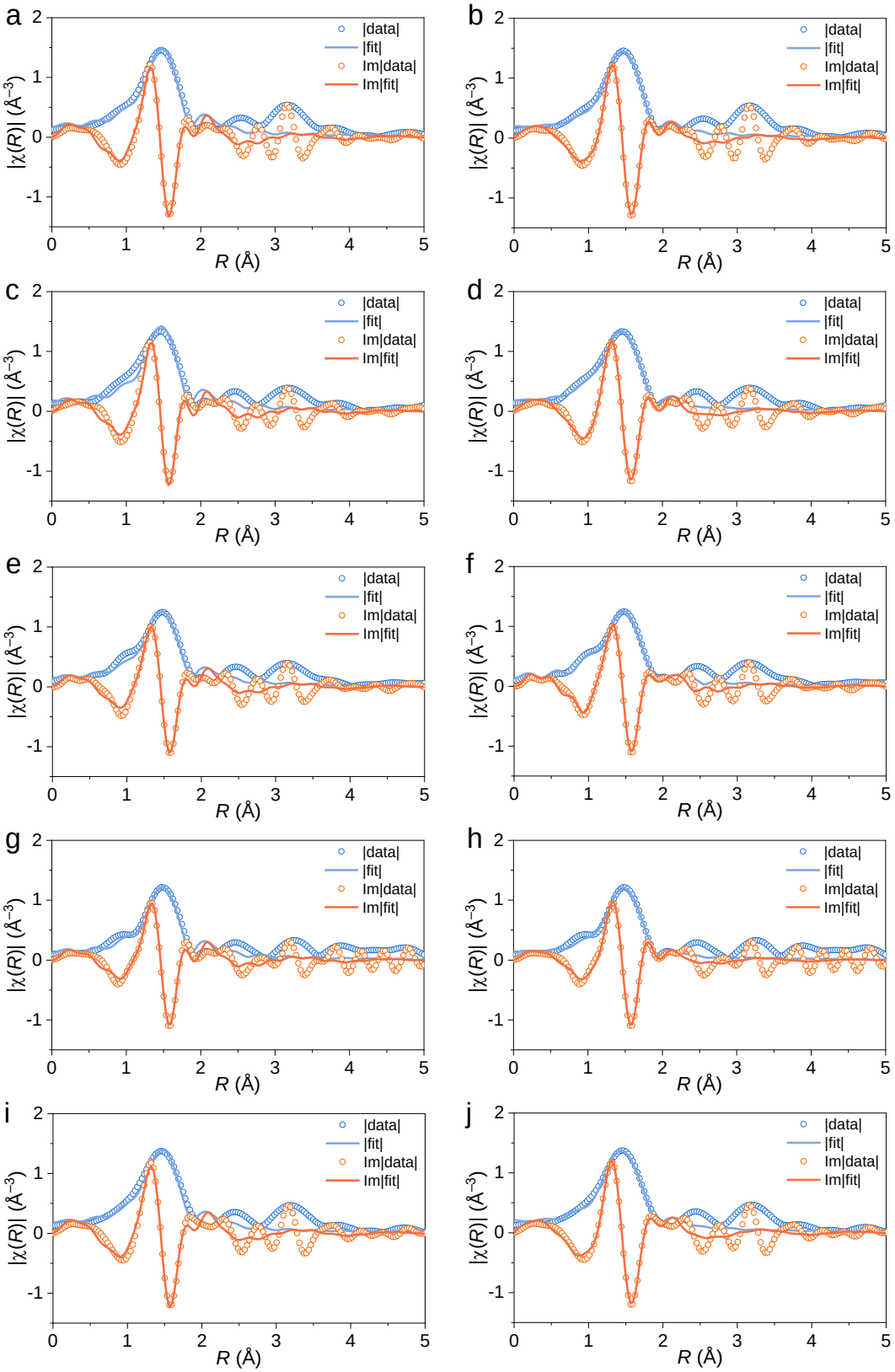

Figure R33 | The Fourier-transform EXAFS spectra (magnitude and imaginary part) for L2-Cu at the Cu *k*-edge. The corresponding EXAFS fits were based on single Cu–N scatter path (**a, c, e, g, i**) and mixed

Cu–C/N/O scatter paths (**b, d, f, h, j**), respectively, showing the magnitude (experimental data: blue circles; fitting data: blue lines) and imaginary portions (experimental data: orange circles; fitting data: orange lines) of Fourier transforms of the data. The *k*-range of 2.5–11 $Å^{-1}$ and the *R*-range of 0–2.2 Å were used for the fits. **a** and **b**, at OCP before reaction; **c** and **d**, at –0.69 V; **e** and **f**, at –0.73 V; **g** and **h**, at –0.79 V; **i** and **j**, at OCP after reaction.

Table R3 | EXAFS fitting results for L2-Cu before, during, and after CO_2RR. Single Cu–N scatter path (blue rows) and mixed Cu–C/N/O scatter paths (orange rows), respectively, have been applied to fit the data. Data range *k* = 2.5–11 $Å^{-1}$, amplitude reaction factor S_0^2 = 0.8, bond distance *R* = 0–2.2 Å. CN: Coordination numbers. *R*: bond distances. ΔE: The inner potential shift. σ^2: The Debye-Waller factor.

	Scatter path	CN	*R* (Å)	ΔE (eV)	σ^2 ($Å^2$)	R-factor
OCP before reaction	Cu–N	2.0(8)	2.00	2.4	0.00471	0.58%
	Cu–O	2.0(6)	1.84	2.4	0.00295	
	Cu–N	5.0(8)	1.94	2.9	0.00369	2.87%
–0.69 V	Cu–N	1.8(5)	1.82	–0.6	0.00672	1.07%
	Cu–O	1.5(4)	1.89	–0.6	0.00580	
	Cu–C	0.7(9)	2.06	–0.6	0.01055	
	Cu–N	4.3(2)	1.93	2.6	0.00233	4.88%
–0.73 V	Cu–N	1.9(3)	1.82	0.2	0.00383	1.03%
	Cu–O	1.0(5)	1.89	0.2	0.00938	
	Cu–C	0.9(2)	2.07	0.2	0.01122	
	Cu–N	4.4(4)	1.94	3.5	0.00414	3.38%
–0.79 V	Cu–N	2.0(9)	1.88	4.1	0.00366	0.94%
	Cu–O	1.3(4)	2.03	4.1	0.00626	
	Cu–C	1.0(7)	2.38	4.1	0.00257	
	Cu–N	3.7(2)	1.94	3.9	0.00241	3.08%
OCP after reaction	Cu–N	2.1(7)	2.01	2.8	0.00369	1.38%
	Cu–O	2.1(2)	1.84	2.8	0.00355	
	Cu–N	5.3(9)	1.93	2.8	0.00517	4.10%

We have now fitted the data up to 4 Å with three distances. The fitting results are shown in Figure R34 and Tables R4–R8. The high consistency between fitting and experimental data warrants integrity of our efforts in using EXAFS for mechanistic analyses.

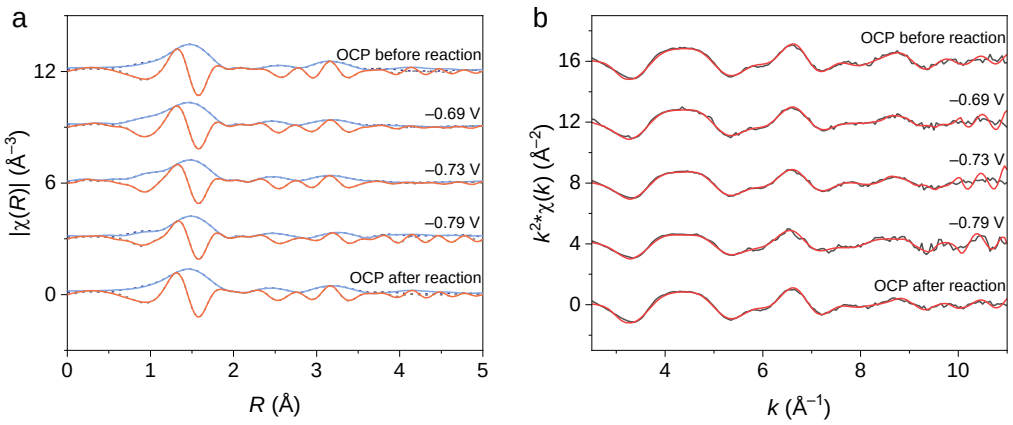

Figure R34 (now added as Supplementary Fig. 26 and 27 in SI) | The *operando* FT-EXAFS spectra fitting results. a, The *operando* Fourier-transform EXAFS spectra (magnitude and imaginary part) for **L2**-Cu at the Cu *k*-edge, showing the magnitude (experimental data: blue circles; fitting data: blue lines) and imaginary portions (experimental data: orange circles; fitting data: orange lines). . The *k*-range of 2.5–11 $Å^{-1}$ and the *R*-range of 0–4 Å were used for the fits. **b,** EXAFS spectra in *k*-space at the Cu *k*-edge. Experimental data: dark grey; fitting data: red.

Table R4 (now added as Supplementary Table 1 in SI) | Interatomic distances and coordination numbers determined by EXAFS analysis of L2-Cu under OCP state before CO_2RR. Data range *k* = 2.5–11 $Å^{-1}$, amplitude reaction factor S_0^2 = 0.8, bond distance *R* = 0–4 Å. CN: Coordination numbers. ΔE: The inner potential shift. σ^2: The Debye-Waller factor. First shell: yellow lines; Second shell: blue lines; Third shell: green lines.

	Scatter path	CN	*R* (Å)	ΔE (eV)	σ^2 ($Å^2$)	R-factor
OCP before reaction	Cu–O	2.00	1.83	1.2	0.00297	0.64%
	Cu–N	2.00	1.99	1.2	0.00604	
	Cu–N	2.05	2.88	1.2	0.01202	
	Cu–C	2.03	3.16	1.2	0.0150	
	Cu–C	1.02	3.35	1.2	0.03102	
	Cu–Cu	2.06	3.11	1.2	0.00906	
	Cu–C	1.02	3.22	1.2	0.03088	
	Cu–N	1.02	3.37	1.2	0.02305	
	Cu–N	1.01	4.09	1.2	0.02610	
	Cu–C	2.02	4.28	1.2	0.02313	

Table R5 (now added as Supplementary Table 6 in SI) | Interatomic distances and coordination numbers determined by EXAFS analysis of L2-Cu at –0.69 V. Data range *k* = 2.5–11 $Å^{-1}$, amplitude reaction factor

S_0^2 = 0.8, bond distance R = 0–4 Å. CN: Coordination numbers. ΔE: The inner potential shift. σ^2: The Debye-Waller factor. First shell: yellow lines; Second shell: blue lines; Third shell: green lines.

	Scatter path	CN	*R* (Å)	ΔE (eV)	σ^2 (Å^2)	R-factor
–0.69 V	Cu–N	2.00	2.05	3.7	0.00907	0.30%
	Cu–C	1.00	1.93	3.7	0.00791	
	Cu–O	1.00	1.78	3.7	0.00514	
	Cu–O	0.99	3.05	3.7	0.0191	
	Cu–N	0.99	2.92	3.7	0.01492	
	Cu–C	1.00	2.34	3.7	0.01487	
	Cu–C	1.98	3.30	3.7	0.02531	
	Cu–N	1.00	3.45	3.7	0.02918	
	Cu–C	0.99	3.50	3.7	0.03207	
	Cu–Cu	1.00	3.25	3.7	0.02085	
	Cu–C	1.00	3.41	3.7	0.03777	
	Cu–Cu	1.01	3.89	3.7	0.01046	

Table R6 (now added as Supplementary Table 7 in SI) | Interatomic distances and coordination numbers determined by EXAFS analysis of L2-Cu at –0.73 V. Data range k = 2.5–11 Å^{-1}, amplitude reaction factor S_0^2 = 0.8, bond distance R = 0–4 Å. CN: Coordination numbers. ΔE: The inner potential shift. σ^2: The Debye-Waller factor. First shell: yellow lines; Second shell: blue lines; Third shell: green lines.

	Scatter path	CN	*R* (Å)	ΔE (eV)	σ^2 (Å^2)	R-factor
–0.73 V	Cu–N	2.00	2.06	4.4	0.0141	0.24%
	Cu–C	1.00	1.94	4.4	0.01089	
	Cu–O	1.00	1.79	4.4	0.00630	
	Cu–O	1.00	2.93	4.4	0.02093	
	Cu–N	1.00	3.09	4.4	0.01932	
	Cu–C	0.99	2.38	4.4	0.01038	
	Cu–C	1.98	3.39	4.4	0.01953	
	Cu–N	1.01	3.47	4.4	0.02127	
	Cu–C	1.00	3.46	4.4	0.01568	
	Cu–Cu	1.01	3.27	4.4	0.02247	
	Cu–C	1.01	3.44	4.4	0.01650	
	Cu–Cu	1.03	3.90	4.4	0.00650	

Table R7 (now added as Supplementary Table 8 in SI) | Interatomic distances and coordination numbers determined by EXAFS analysis of L2-Cu at –0.79 V. Data range k = 2.5–11 Å^{-1}, amplitude reaction factor S_0^2 = 0.8, bond distance R = 0–4 Å. CN: Coordination numbers. ΔE: The inner potential shift. σ^2: The Debye-Waller factor. First shell: yellow lines; Second shell: blue lines; Third shell: green lines.

	Scatter path	CN	*R* (Å)	ΔE (eV)	σ^2 (Å^2)	R-factor
–0.79 V	Cu–N	2.01	1.97	4.7	0.00501	0.77%
	Cu–C	1.04	2.16	4.7	0.00248	
	Cu–O	1.00	1.82	4.7	0.00358	
	Cu–O	1.08	2.86	4.7	0.01793	
	Cu–N	1.09	3.06	4.7	0.02924	
	Cu–C	1.09	3.21	4.7	0.03324	
	Cu–C	2.19	3.31	4.7	0.02514	
	Cu–N	1.08	3.51	4.7	0.03591	
	Cu–C	1.09	3.60	4.7	0.03693	
	Cu–Cu	1.09	3.34	4.7	0.02749	
	Cu–C	1.08	3.46	4.7	0.03816	
	Cu–Cu	1.07	3.69	4.7	0.00985	

Table R8 (now added as Supplementary Table 9 in SI) | Interatomic distances and coordination numbers determined by EXAFS analysis of L2-Cu under OCP after CO_2RR. Data range k = 2.5–11 Å^{-1}, amplitude reaction factor S_0^2 = 0.8, bond distance R = 0–4 Å. CN: Coordination numbers. ΔE: The inner potential shift. σ^2: The Debye-Waller factor. First shell: yellow lines; Second shell: blue lines; Third shell: green lines.

	Scatter path	CN	*R* (Å)	ΔE (eV)	σ^2 (Å^2)	R-factor
OCP after reaction	Cu–O	2.00	1.82	1.2	0.00407	0.57%
	Cu–N	2.00	1.99	1.2	0.00741	
	Cu–N	2.02	2.87	1.2	0.01192	
	Cu–C	2.03	3.22	1.2	0.02749	
	Cu–C	1.01	3.28	1.2	0.02960	
	Cu–Cu	2.03	3.10	1.2	0.01217	
	Cu–C	1.02	3.05	1.2	0.01810	
	Cu–N	1.01	3.37	1.2	0.03094	
	Cu–N	1.01	4.11	1.2	0.02602	
	Cu–C	2.02	4.29	1.2	0.02336	

12. Suppl Fig 4: Are the Cu LMM spectra - Auger? If so, please mention it. In the caption, "X-Cu" probably means Ln-Cu? Please make this wording consistent.

Reply: We have revised the caption of Supplementary Fig 6 to "Supplementary Fig. 6 | Cu 2*p* XPS (bottom) and Auger Cu *LMM* (up) spectra of **Ln**-Cu."

13. Page 7 Lines 8-9 and Suppl Fig 12: what catalyst was used for the MEA long-term testing?

Reply: We have supplemented the information to the caption of Supplementary Fig 15 to "Supplementary Fig. 15 | CO_2RR performance test of **L2**-Cu in the MEA system."

14. Figures in general: Why do the authors only show one structure in the manuscript and the rest in SupplInfo? Please reconsider this because the reader wants to see data for all the samples mentioned.

Reply: To provide clearer and more comprehensive information of the coordination polymer structures, we have now updated the Fig. 2e as Figure R35. We illustrate the general molecular structure using **L2**-Cu as an example and depict the molecular structures of all the substituents alongside. The rationale is all the **Ln**-Cu catalysts share the similar packing structure according to PXRD patterns.

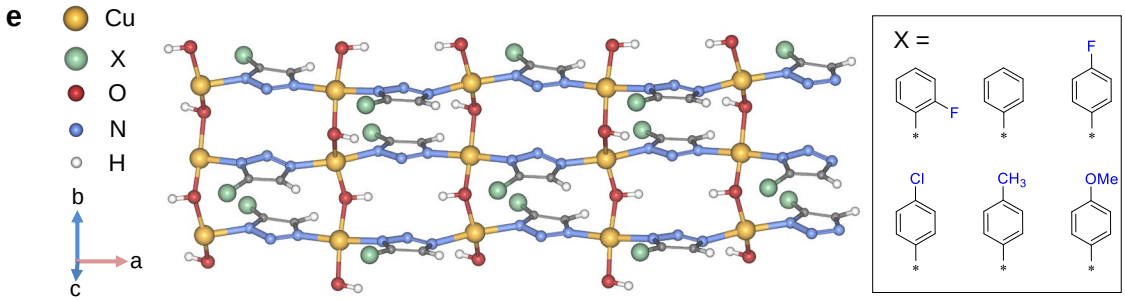

Figure R35 (now updated as Fig. 2e in MS) | The structure of Ln-Cu. X represents the substituents and is on the right frame. * indicates the position connecting with triazole rings.

15. Suppl Fig 14: Photo at beamline: please explain what the reader is looking at. Label the main components (ion chambers, fluorescence detector, cell, potentiostat, electrolyte flow in/out); draw the X-ray beam path.

Reply: We have added annotations to the photographs (Figure R36).

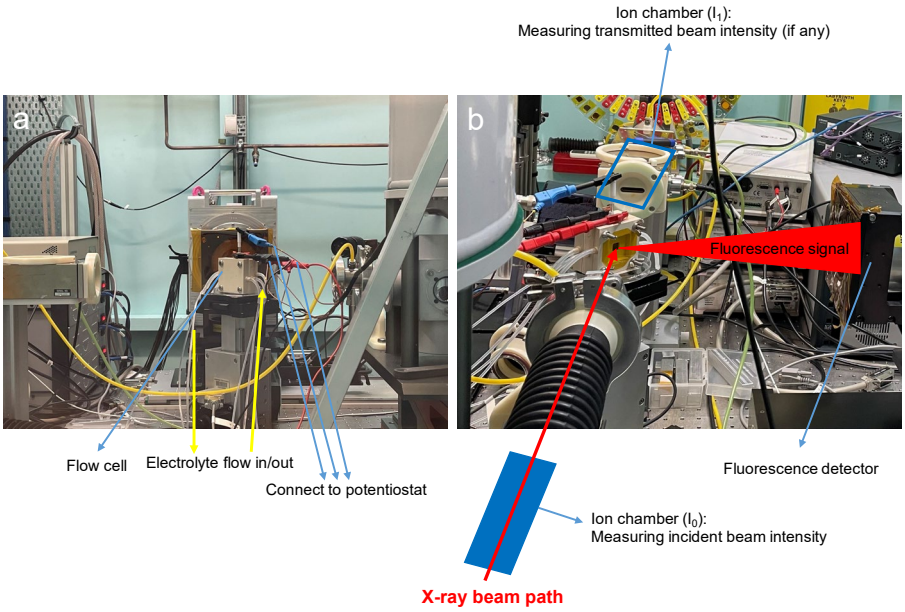

Figure R36 (now updated as Supplementary Fig. 23 in SI) | The photograph of *operando* XAS experiments in operation. a, Front view. **b,** Side view. The yellow arrows show the electrolyte flow direction. The red arrows show the X-ray beam path.

16. The Methods section mentions SEM - is that data shown?

Reply: SEM images are now included in the revised Supplementary Information, and we updated accordingly the *Methods*, writing: The morphologies of samples were recorded by SEM (Zeiss Sigma VP 3view). SEM-EDS mapping was mapped by Zeiss Sigma VP HD.

17. Fig 1 (c): Please invert y-axis for proper orientation.

Reply: We have inverted y-axis of Fig. 1c in the revise manuscript (Figure R37).

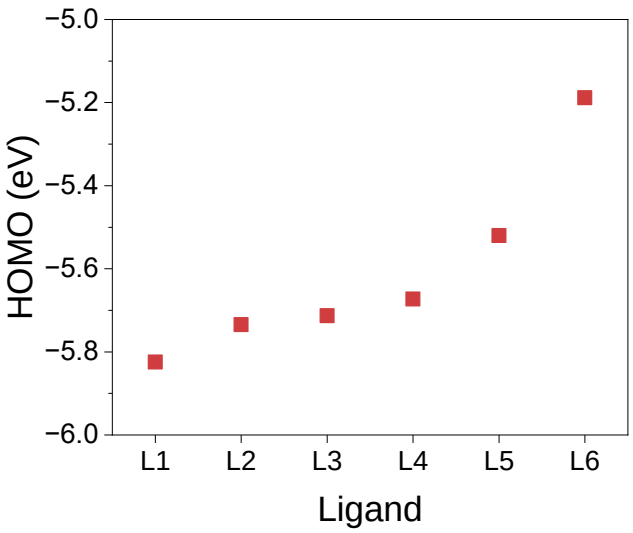

Figure R37 (now updated as Fig. 1c in MS) | HOMO energy of ligand. The anionic form of ligands rather than neutral form was used for the calculation due to deprotonation.

18. For the word *operando* please use italics.

Reply: We have revised all operando to "*operando*" throughout main text and SI.

19. In Methods: incorrectly printed character "-" for inverse units, i.e. mg cm-1, mL min-1, etc.

Reply: We have now corrected this throughout main text and SI.

20. Page 9 Line 7 and Fig 4 (b): Please use subscripts for molecules FE_{C_{2+}} and FE_{CH_{4}} .

Reply: We have fixed this now.

21. Fig 4 (d): Please use proper label i.e. U = -0.93 +/- 0.01 V (no "@" etc), and use consistent precision (either 2 or 3 decimal places).

Reply: We have corrected the label to "E = –0.930 ± 0.008 V" shown in updated Fig. 4d in the main text.

22. Fig 5: please use proper legends/labels in the figures for the curves. The "color scale" is really confusing and illegible in black/white print.

Reply: We have revised the legends in Fig. 5 in the revised manuscript.

23. References: Please use full author list. Include DOI if required.

Reply: We have revised the references with full author list and DOI added.

REVIEWER COMMENTS

Reviewer #1 (Remarks to the Author):

The authors have addressed all points, therefore the work is suitable for acceptance in nature communication.

Reviewer #2 (Remarks to the Author):

Most of the comments were addressed, however there are still concerns in conclusive phrasing that cannot be not supported by the technique or analysis of select spectroscopy. Please see below for further questions/modification requests.

RE:RE: 1: In response to my question: “EXAFS is not sensitive enough to assert the single-site nature of a material. Can the authors comment on this considering this new understanding of EXAFS limitations?” the authors wrote an acknowledgement of the problem (in the review) and went on to do operando EXAFS fitting. While the additional fitting is interesting, in the paper that I cited, authors noted that “Ultimately, we argue that it is extremely valuable to directly compare the quality of fits for models containing the proposed SAC structure and the antithesis –models of metal oxide or metal clusters.”. For example, this paper: https://onlinelibrary.wiley.com/doi/full/10.1002/anie.201912857 demonstrates that even with clear nanoparticles (seen by XRD), the EXAFS fits to a nominal single-atom-catalyst motif.

Therefore, I will rephrase the question/request: In the manuscript, can the authors comment on the limit of detection of nanoparticles/clusters? Ideally, the authors will confirm not only lack of change in the bulk (as they have done with operando comparisons) but validate their initial structure with EXAFS in comparison to fits to small clusters. Furthermore, phrasing on this topic will also need to be updated in the text, for example, this sentence “Using operando X-ray absorption spectroscopy (XAS) and in-situ infrared (IR) spectroscopy, we confirmed that all these catalysts were stable and remained as single sites during CO2RR catalysis”. Neither XAS nor IR spectroscopy can confirm that these materials are 100% single-sites and they are both bulk techniques and would not be suitable to assert that all the sites remained unchanged. Please update all similar phrases to be more precise, e.g. “operando XAS/in situ IR support the hypothesis that there are no bulk material changes under applied potential”.

Lastly, it is unclear how the additional in-situ Raman or SEM help answer the question of the catalysts being SAC, please either explain how this is possible, or rephrase.

RE:RE:2 – This concern was addressed.

RE:RE:3 – This concern was addressed.

RE:RE:4. Thank you for the addition of further XRD. This concern was addressed.

RE:RE:5. Thank you for the addition of extra information and cell schematics. This concern was addressed.

RE:RE:6: Thank you for the addition of the table and post characterization and reversibility question. Commenting further on the spectroscopy, I have a couple of follow-up questions:

1) “The recovered *CO absorption intensity and peak positions indicate the stability of the Catalysts” Can the authors explain this, specifically, if their catalysts do degrade, what would they expect to see in the cases where small Cu clusters begin to form? Or how would the authors imagine degradation in their systems and why could this be tracked by the *CO?

2) “post-reaction spectra were added to Supplementary Fig. 34, which showed almost the same signals (position and intensity) as those before reaction, indicating stable structure of Ln-Cu catalysts” This is a very qualitative assessment. I would suggest to be more quantitative here and specify what regions, as a) figure S34 does not show pre/post characterization, just post characterization to in situ samples (perhaps do a difference spectra if you want to make this claim) and b) by eye there do appear to be substantial changes to FWHM and peak ratios.

RE:RE:7 – This concern was addressed.

RE:RE:8 – This concern was addressed.

Reviewer #3 (Remarks to the Author):

The authors reviewed the paper very thoroughly and replied to all questions. I recommend this manuscript for publication. However, I have two points that should be re-visited first.

Reviewer 3, Comment 5. Page 8, Line 17: The HOMO level...

Thanks for the clarification about the bonding of CO to Cu2+ and the additional citation (J. Am. Chem. Soc. 1985, 107, 578-584). Can the authors add this last sentence to the manuscript?

Reviewer 3, Comment 11.5: EXAFS model

Thanks for the re-work of the single-shell versus multiple-shell fit. The slight improvement of the fit possibly indicates that the shell is split, and 2-3 bond distances can be refined, which the authors have well demonstrated. However, the initial reviewer comment is still valid, in that neighboring-Z back-scatterers cannot be distinguished. Therefore, the authors must clearly state that the assignment of N/O/C back-scatterers is subjective, and is based on the prior knowledge of the structure, e.g. the interatomic distances are consistent with DFT.

The final fits (e.g. operando EXAFS) look really good, but there is a caveat. When making the model more detailed, e.g. by adding more shells and parameters, the errors of the individual parameters can increase significantly. Can the authors indicate errors for all the determined parameters, not only coordination numbers? Since the compounds here have a well-defined and well-known molecular structure, high errors are not a problem, and are more a measure of the sensitivity of the EXAFS technique itself. This should be briefly mentioned in the manuscript.

Response Letter

We thank the editor and all reviewers for the comments, which help us improve the quality of this manuscript. Below we respond to each reviewer's remarks point by point.

Reviewer's comments are in blue and the changes we made in the manuscript are in green.

Reviewer #1:

The authors have addressed all points, therefore the work is suitable for acceptance in nature communication.

Reply: We sincerely thank this reviewer for the comments and suggestions which has helped improve the quality of this work.

Reviewer #2:

Most of the comments were addressed, however there are still concerns in conclusive phrasing that cannot be not supported by the technique or analysis of select spectroscopy. Please see below for further questions/modification requests.

Reply: We sincerely thank the reviewer for the recommendation. The point-by-point reply is below.

RE:RE: 1: In response to my question: "EXAFS is not sensitive enough to assert the single-site nature of a material. Can the authors comment on this considering this new understanding of EXAFS limitations?" the authors wrote an acknowledgement of the problem (in the review) and went on to do operando EXAFS fitting. While the additional fitting is interesting, in the paper that I cited, authors noted that "Ultimately, we argue that it is extremely valuable to directly compare the quality of fits for models containing the proposed SAC structure and the antithesis —models of metal oxide or metal clusters.". For example, this paper: https://onlinelibrary.wiley.com/doi/full/10.1002/anie.201912857 demonstrates that even with clear nanoparticles (seen by XRD), the EXAFS fits to a nominal single-atom-catalyst motif.

Therefore, I will rephrase the question/request: In the manuscript, can the authors comment on the limit of detection of nanoparticles/clusters? Ideally, the authors will confirm not only lack of change in the bulk (as they have done with operando comparisons) but validate their initial structure with EXAFS in comparison to fits to small clusters. Furthermore, phrasing on this topic will also need to be updated in the text, for example, this sentence "Using operando X-ray absorption spectroscopy (XAS) and in-situ infrared (IR) spectroscopy, we

confirmed that all these catalysts were stable and remained as single sites during CO2RR catalysis". Neither XAS nor IR spectroscopy can confirm that these materials are 100% single-sites and they are both bulk techniques and would not be suitable to assert that all the sites remained unchanged. Please update all similar phrases to be more precise, e.g. "operando XAS/in situ IR support the hypothesis that there are no bulk material changes under applied potential".

Lastly, it is unclear how the additional in-situ Raman or SEM help answer the question of the catalysts being SAC, please either explain how this is possible, or rephrase.

Reply: In the revised manuscript (page 7), we have commented the EXAFS limit of detecting nanoparticles/clusters and added the proceeding sentence to provide context: It is acknowledged that small number of clusters might exist due to the limit of detection of EXAFS technique (*ACS Catal.* 2023, 13, 6462–6473).

Besides, we have re-phrased the descriptions of materials towards each technique to be more precise:

Page 4 in MS: *Operando* X-ray absorption spectroscopy (XAS) and *in-situ* infrared (IR) spectroscopy support that there is no bulk material change under applied potentials relevant to CO_2RR.

Page 8 in MS: These results indicated the predominant presence of single-site Cu atoms in **L2**-Cu catalysts under applied potentials, serving as the active sites for binding CO_2RR reactants and intermediates.

We have validated the structural configuration of **L2**-Cu using EXAFS and compared it with fits to small clusters. DFT was employed to simulate the structures of **L2**-Cu_2 and **L2**-Cu_3, which are models consisting of small clusters with two and three Cu atoms, respectively (Figure R1). We have fitted and compared the FT-EXAFS of **L2**-Cu at OCP state using the simulated structures (Figure R2). While the R-factor does not cross or merely overshoot the artificial 1% "good fit" threshold set in the reference (*ACS Catal.* 2023, 13, 6462–6473), the Cu–Cu metal distances in **L2**-Cu, **L2**-Cu_2, and **L2**-Cu_3 are 3.11 Å, 2.25 Å, and 2.18 Å, separately (Tables R1–R3), with the latter two significantly exceeding the Cu–Cu metal distance of 2.55 Å in a standard Cu metal model. This suggests an unreasonable fitting using the **L2**-Cu_2 and **L2**-Cu_3 models. Besides, the fitting with **L2**-Cu model yielded the lowest R-factor of 0.64%, compared to 0.71% for **L2**-Cu_2 and 1.45% for **L2**-Cu_3. Hence, we believe the single-site Cu model showed the best fitting.

We have updated on page 6 in MS: Further, single-site Cu showed the best fitting results in comparison with Cu clusters and no metallic Cu–Cu bond was identified (Supplementary Figs. 7–9 and Supplementary Tables 1–3).

We also explained in detail on page 12 in SI: The fitting results showed that the Cu–Cu metal distances in **L2**-Cu, **L2**-Cu_2, and **L2**-Cu_3 are 3.11 Å, 2.25 Å, and 2.18 Å, separately (Supplementary Tables 1–3). The standard Cu metal foil model indicates a Cu–Cu metal distance of 2.55 Å, significantly greater than the distances in **L2**-Cu_2 or **L2**-Cu_3, suggesting an unreasonable fitting of **L2**-Cu catalyst using either **L2**-Cu_2 or **L2**-Cu_3 model.

Besides, the fitting with **L2**-Cu model yielded the lowest R-factor of 0.64%, compared to 0.71% for **L2**-Cu_2 and 1.45% for **L2**-Cu_3, indicating that the **L2**-Cu single-site model showed the best fitting result.

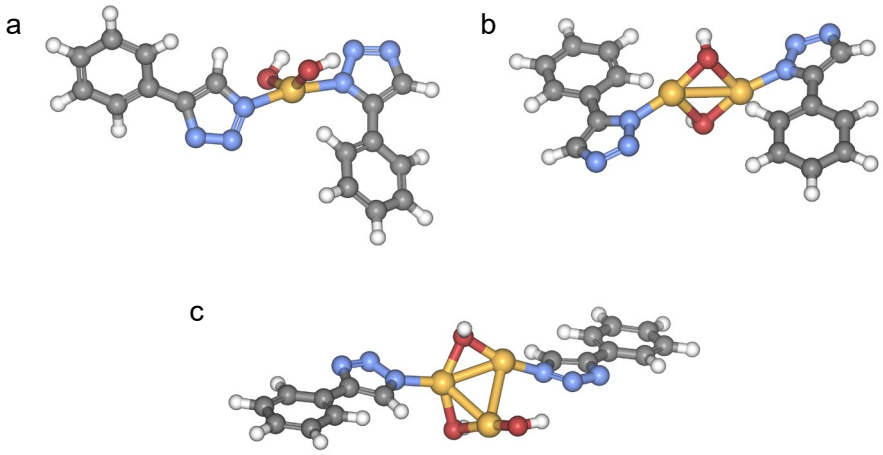

Figure R1 (now added as Supplementary Fig. 8 in SI) | L2-Cu (a), L2-Cu_2 (b), and L2-Cu_3 (c) models used for FT-EXAFS fitting.

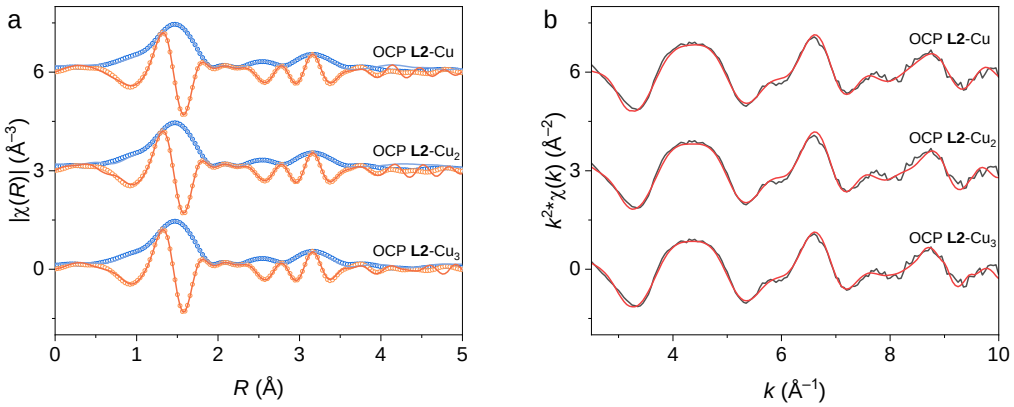

Figure R2 (now added as Supplementary Fig. 9 in SI) | The FT-EXAFS spectra fitting results for L2-Cu at OCP state with L2-Cu, L2-Cu_2, and L2-Cu_3 models. a, The Fourier-transform EXAFS spectra (magnitude and imaginary part) for **L2**-Cu at OCP state fitted with **L2**-Cu, **L2**-Cu_2, and **L2**-Cu_3 models at the Cu *k*-edge, showing the magnitude (experimental data: blue circles; fitting data: blue lines) and imaginary portions (experimental data: orange circles; fitting data: orange lines). The *k*-range of 2.5–10 $Å^{-1}$ and the *R*-range of 0–4 Å were used for the fits. **b,** EXAFS spectra in *k*-space at the Cu *k*-edge. Experimental data: dark grey; fitting data: red. The fitting results showed that the Cu–Cu metal distances in **L2**-Cu, **L2**-Cu_2, and **L2**-Cu_3 are 3.11 Å, 2.25 Å, and 2.18 Å, separately (Supplementary Tables 1–3). The standard Cu metal foil model indicates a Cu–Cu metal distance of 2.55 Å, significantly greater than that distance in **L2**-Cu_2 or **L2**-Cu_3, meaning the unreasonable fitting of **L2**-Cu catalyst using **L2**-Cu_2 and **L2**-Cu_3 models. Besides, the fitting with **L2**-Cu model

yielded the lowest R-factor of 0.64%, compared to 0.71% for **L2**-Cu_2 and 1.45% for **L2**-Cu_3, indicating that the **L2**-Cu single-site model showed the best fitting result.

Table R1 (now updated as Supplementary Table 1 in SI) | Interatomic distances and coordination numbers determined by EXAFS analysis of L2-Cu under OCP state before CO_2RR using L2-Cu model. Data range k = 2.5–11 $Å^{-1}$, amplitude reaction factor S_0^2 = 0.8, bond distance R = 0–4 Å. CN: Coordination numbers. ΔE: The inner potential shift. σ^2: The Debye-Waller factor. First shell: yellow lines; Second shell: blue lines; Third shell: green lines.

	Scatter path	CN	*R* (Å)	ΔE (eV)	σ^2 ($Å^2$)	R-factor
L2-Cu at OCP	Cu–O	2.00±0.06	1.83±0.12	1.2±0.4	0.00297±0.00371	0.64%
	Cu–N	2.00±0.06	1.99±0.01	1.2±0.4	0.00604±0.00386	
	Cu–N	2.05±0.23	2.88±0.07	1.2±0.4	0.01202±0.00585	
	Cu–C	2.03±0.21	3.16±0.15	1.2±0.4	0.0150±0.01146	
	Cu–C	1.02±0.11	3.35±0.24	1.2±0.4	0.03102±0.00644	
	Cu–Cu	2.06±0.33	3.11±0.27	1.2±0.4	0.00906±0.00411	
	Cu–C	1.02±0.12	3.22±0.19	1.2±0.4	0.03088±0.01241	
	Cu–N	1.02±0.11	3.37±0.36	1.2±0.4	0.02305±0.03155	
	Cu–N	1.01±0.09	4.09±0.25	1.2±0.4	0.02610±0.02044	
	Cu–C	2.02±0.20	4.28±0.37	1.2±0.4	0.02313±0.01972	

Table R2 (now added as Supplementary Table 2 in SI) | Interatomic distances and coordination numbers determined by EXAFS analysis of L2-Cu under OCP state before CO_2RR using L2-Cu_2 model. Data range k = 2.5–10 $Å^{-1}$, amplitude reaction factor S_0^2 = 0.8, bond distance R = 0–4 Å. CN: Coordination numbers. ΔE: The inner potential shift. σ^2: The Debye-Waller factor. First shell: yellow lines; Second shell: blue lines; Third shell: green lines.

	Scatter path	CN	*R* (Å)	ΔE (eV)	σ^2 ($Å^2$)	R-factor
L2-Cu_2 at OCP	Cu-O	1.01±0.03	1.77±0.02	3.1±2.3	0.01406±0.00456	0.71%
	Cu-O	1.01±0.03	1.90±0.01	3.1±2.3	0.01938±0.00501	
	Cu-N	1.02±0.06	2.05±0.11	3.1±2.3	0.02199±0.00261	
	Cu-Cu	1.04±0.11	2.25±0.27	3.1±2.3	0.01110±0.01034	
	Cu-N	1.03±0.11	2.44±0.41	3.1±2.3	0.02092±0.01236	
	Cu-C	1.01±0.07	2.92±0.05	3.1±2.3	0.01448±0.00589	
	Cu-N	1.00±0.05	4.17±0.17	3.1±2.3	0.03350±0.00430	
	Cu-N	1.01±0.06	4.03±0.06	3.1±2.3	0.03038±0.00391	
	Cu-C	1.01±0.05	4.34±0.24	3.1±2.3	0.03171±0.00441	

Table R3 (now added as Supplementary Table 3 in SI) | Interatomic distances and coordination numbers determined by EXAFS analysis of L2-Cu under OCP state before CO_2RR using L2-Cu_3 model. Data range

k = 2.5–10 Å^{-1}, amplitude reaction factor S_0^2 = 0.8, bond distance R = 0–4 Å. CN: Coordination numbers. ΔE: The inner potential shift. σ^2: The Debye-Waller factor. First shell: yellow lines; Second shell: blue lines; Third shell: green lines.

	Scatter path	CN	R (Å)	ΔE (eV)	σ^2 (Å^2)	R-factor
L2-Cu_3 at OCP	Cu-N	1.00±0.02	1.96±0.11	1.4±6.6	0.03009±0.01000	0.71%
	Cu-O	1.00±0.02	1.78±0.07	1.4±6.6	0.02176±0.00933	
	Cu-Cu	1.00±0.02	2.18±0.29	1.4±6.6	0.02252±0.01545	
	Cu-Cu	1.00±0.03	2.43±0.24	1.4±6.6	0.02204±0.02644	
	Cu-N	1.00±0.03	2.61±0.19	1.4±6.6	0.03177±0.02290	
	Cu-C	1.00±0.03	2.38±0.44	1.4±6.6	0.03067±0.04030	
	Cu-O	1.00±0.12	2.90±0.32	1.4±6.6	0.00937±0.08337	
	Cu-O	0.98±0.28	3.68±0.18	1.4±6.6	0.00678±0.11241	
	Cu-N	0.99±0.03	4.16±0.25	1.4±6.6	0.03508±0.01269	
	Cu-C	1.01±0.03	4.33±0.37	1.4±6.6	0.03208±0.01307	
	Cu-N	0.99±0.03	4.01±0.31	1.4±6.6	0.03263±0.01412	

In-situ Raman and SEM analyses serve as supplementary evidence for elucidating the single-site nature of the catalysts. The Raman signals originating from organic molecules suggest the retention of ligands on the gas diffusion electrode (GDE) surface. SEM images indicate that the morphology of the bulk materials did not undergo significant changes. To make the description more precise and avoid over-interpretation, we have revised the wording in both MS and SI:

On page 12 in MS: The spectra obtained during and after the reaction indicated the retention of ligands on the electrode surface (Supplementary Figs. 36–42).

On page 39 in SI: The post-reaction spectra indicate the retention of ligands after *in-situ* Raman test.

RE:RE:6: Thank you for the addition of the table and post characterization and reversibility question. Commenting further on the spectroscopy, I have a couple of follow-up questions:

1) "The recovered *CO absorption intensity and peak positions indicate the stability of the catalysts" Can the authors explain this, specifically, if their catalysts do degrade, what would they expect to see in the cases where small Cu clusters begin to form? Or how would the authors imagine degradation in their systems and why could this be tracked by the *CO?

Reply: *CO intermediates exhibit two modes: $*CO_{atop}$ (located in the range of 2,000–2,100 cm^{-1}) and $*CO_{bridge}$ (located in the range of 1,800–1,900 cm^{-1}) (Figure R3a). If the catalysts undergo degradation, metallic Cu

clusters or nanoparticles should form, allowing adsorbed CO to be observed in the form of $*CO_{bridge}$ (*ACS Catal.* 2018, 8, 7507−7516). Due to the single-site nature of the **Ln**-Cu materials, only $*CO_{atop}$ should be detected, within the limit of detection of IR, during the *in-situ* test (Figure R3b). This phenomenon has been verified by our prior work using the similar coordination polymer Cu catalyst (*Nat. Commun.* 2023, 14, 474), where only $*CO_{atop}$ was detected in single-site catalysts, while both $*CO_{bridge}$ and $*CO_{atop}$ were detected when the catalysts degraded into Cu clusters (Figure R4).

We also updated MS on page 8 for accurate phrases: These results suggested no Cu agglomeration formed to be observable by IR spectroscopy during CO_2RR process.

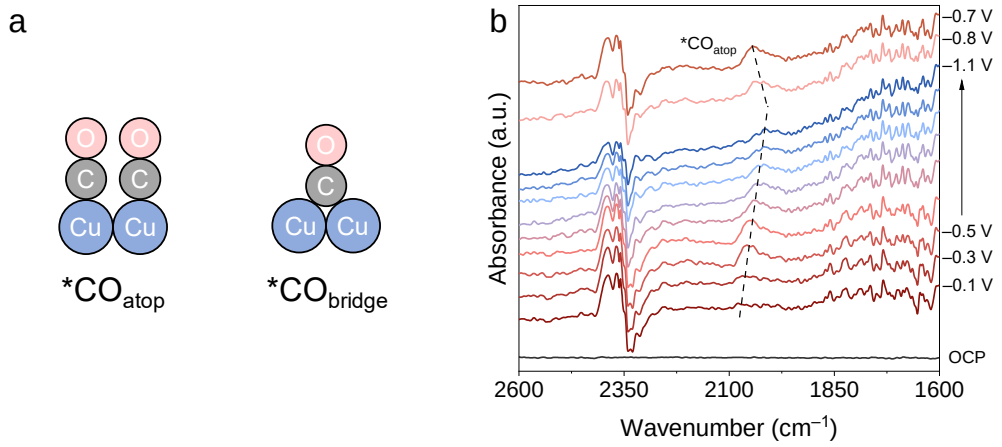

Figure R3 | Different configurations of *CO show different signals in IR spectra. a, $*CO_{atop}$ and $*CO_{bridge}$ configurations. **b,** only $*CO_{atop}$ was observed for **L2**-Cu during *in-situ* IR test.

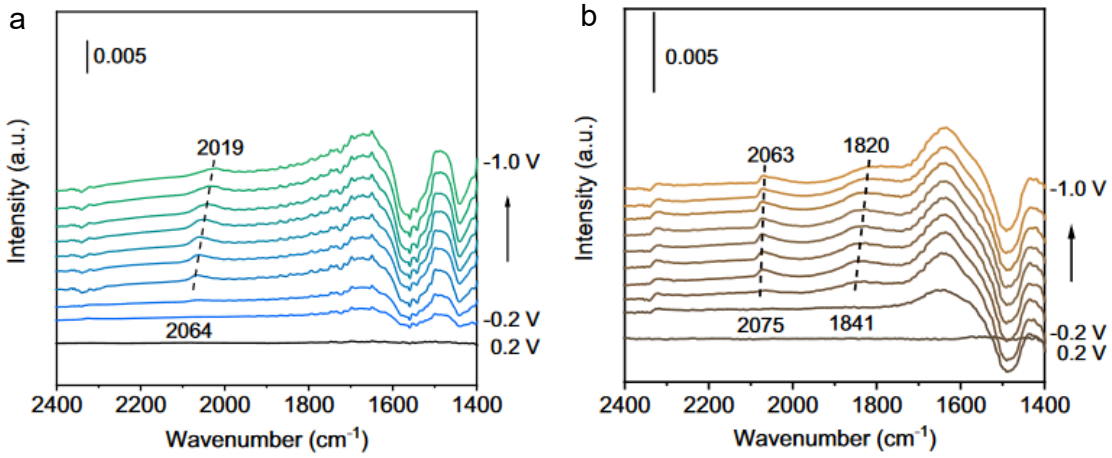

Figure R4 (reproduced from *Nat. Commun.* 2023, 14, 474) | *In-situ* ATR-SEIRAS spectra of a coordination polymer, Cu(OH)BTA, in CO_2–saturated 0.1 M $KHCO_3$ electrolyte. a, Cu(OH)BTA catalysts with single-site nature. **b,** Cu clusters catalysts derived from Cu(OH)BTA.

2) "post-reaction spectra were added to Supplementary Fig. 34, which showed almost the same signals (position and intensity) as those before reaction, indicating stable structure of Ln-Cu catalysts" This is a very qualitative assessment. I would suggest to be more quantitative here and specify what regions, as a) figure S34 does not show pre/post characterization, just post characterization to in situ samples (perhaps do a difference spectra if you want to make this claim) and b) by eye there do appear to be substantial changes to FWHM and peak ratios.

Reply: To give a qualitative assessment, we compared the FWHM, area ratio, and wavenumber of several main peaks for the ligands on the OCP state before and after the reaction. The peak areas were normalized by the area of the highest peak at ~1,600 cm^{-1}. As shown in Figures R5–R10, the peak positions kept almost unchanged. The peaks with relatively high intensities showed similar normalized peak areas and FWHM. The peaks with low intensities exhibited larger variance, which can be ascribed to much lower peak intensities, resulting in lower accuracy of integration of peaks.

We have revised the discussion of *in-situ* Raman spectra (on page 12 in MS): The spectra obtained during and after the reaction indicated the retention of ligands on the electrode surface (Supplementary Figs. 36–42).

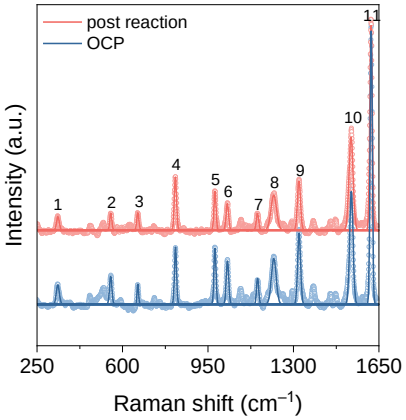

	OCP			Post reaction		
Peak No.	FWHM	Ratio	Wavenumber /cm^{-1}	FWHM	Ratio	Wavenumber /cm^{-1}
1	14.45	0.09	335.14	13.04	0.07	335.61
2	11.48	0.11	551.79	9.99	0.07	552.01
3	7.47	0.05	662.83	10.25	0.07	662.68
4	10.01	0.19	817.11	11.12	0.25	816.71
5	10.18	0.19	978.70	10.26	0.17	978.80
6	12.00	0.18	1029.75	12.17	0.13	1029.35
7	10.28	0.09	1153.19	11.63	0.08	1152.70
8	23.18	0.36	1219.49	26.83	0.39	1219.36
9	14.22	0.35	1323.11	14.85	0.30	1322.75
10	16.46	0.63	1537.09	19.68	0.76	1535.82
11	10.77	1.00	1618.43	11.77	1.00	1617.70

Figure R5 (now added as Supplementary Fig. 37 in SI) | The comparison of Raman spectra of L1-Cu between OCP state and post reaction state. The peak areas were normalized by the area of the highest peak at ~1,600 cm^{-1} (same normalized method for Supplementary Figs. 38–42).

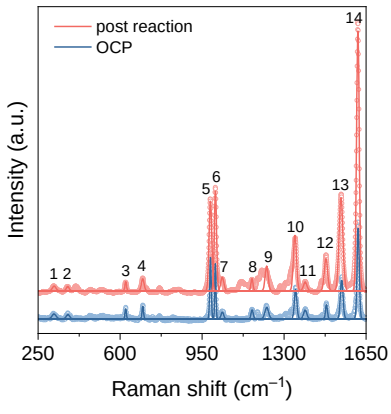

	OCP			Post reaction		
Peak No.	FWHM	Ratio	Wavenumber /cm^{-1}	FWHM	Ratio	Wavenumber /cm^{-1}
1	20.02	0.09	317.99	17.57	0.02	318.53
2	16.64	0.07	377.41	14.40	0.02	376.40
3	6.76	0.07	623.85	8.07	0.02	624.04
4	7.48	0.09	696.83	13.51	0.05	696.75
5	7.66	0.47	985.90	13.66	0.35	985.59
6	6.26	0.34	1006.70	11.30	0.32	1006.99
7	12.84	0.09	1036.66	15.62	0.06	1036.19
8	10.57	0.09	1163.56	10.13	0.04	1162.81
9	18.22	0.20	1226.01	15.31	0.11	1225.69
10	12.72	0.37	1349.31	15.73	0.25	1346.23
11	16.13	0.14	1390.34	17.89	0.04	1390.22
12	9.48	0.13	1480.91	16.77	0.15	1478.86
13	13.37	0.51	1546.00	19.24	0.51	1542.96
14	11.08	1.00	1616.44	13.42	1.00	1615.07

Figure R6 (now added as Supplementary Fig. 38 in SI) | The comparison of Raman spectra of L2-Cu between OCP state and post reaction state.

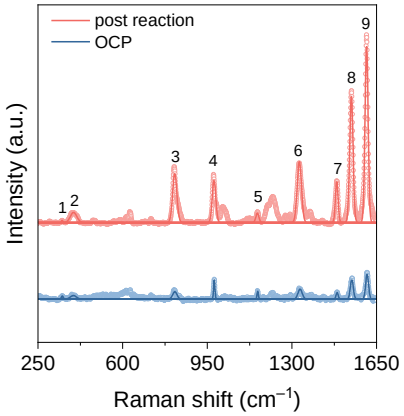

	OCP			Post reaction		
Peak No.	FWHM	Ratio	Wavenumber /cm^{-1}	FWHM	Ratio	Wavenumber /cm^{-1}
1	9.82	0.08	350.70	6.93	0.01	350.00
2	29.16	0.29	396.45	31.29	0.12	397.11
3	20.74	0.44	815.89	20.76	0.38	815.49
4	6.91	0.37	978.95	17.29	0.27	978.00
5	6.54	0.14	1158.43	14.88	0.05	1157.20
6	20.71	0.64	1333.71	20.74	0.51	1330.79
7	10.61	0.19	1486.92	13.20	0.20	1485.40
8	14.75	0.80	1547.71	16.41	0.78	1545.92
9	14.29	1.00	1610.90	15.10	1.00	1608.70

Figure R7 (now added as Supplementary Fig. 39 in SI) | The comparison of Raman spectra of L3-Cu between OCP state and post reaction state.

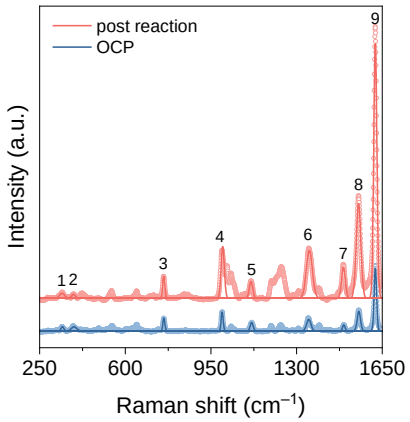

	OCP			Post reaction		
Peak No.	FWHM	Ratio	Wavenumber /cm^{-1}	FWHM	Ratio	Wavenumber /cm^{-1}
1	13.26	0.07	343.10	23.72	0.03	341.71
2	25.97	0.14	390.56	18.39	0.02	388.20
3	9.39	0.16	757.65	10.40	0.06	757.11
4	9.66	0.24	995.78	15.68	0.21	998.14
5	14.10	0.16	1116.54	16.76	0.07	1113.74
6	20.73	0.32	1349.78	28.97	0.35	1352.15
7	12.03	0.09	1492.94	17.57	0.14	1491.53
8	16.07	0.42	1554.39	22.00	0.53	1553.22
9	12.03	1.00	1621.93	15.35	1.00	1621.72

Figure R8 (now added as Supplementary Fig. 40 in SI) | The comparison of Raman spectra of L4-Cu between OCP state and post reaction state.

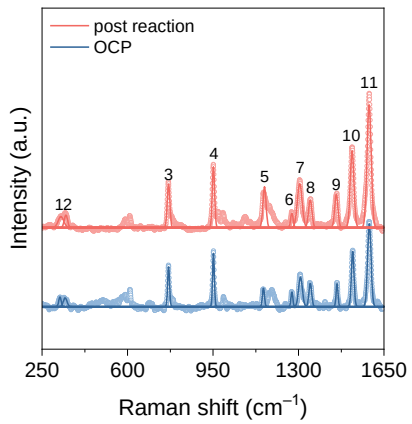

	OCP			Post reaction		
Peak No.	FWHM	Ratio	Wavenumber /cm^{-1}	FWHM	Ratio	Wavenumber /cm^{-1}
1	11.57	0.08	323.26	26.87	0.12	327.34
2	17.37	0.11	344.67	16.02	0.08	347.66
3	9.40	0.27	768.06	12.69	0.22	767.96
4	8.59	0.33	951.87	11.63	0.29	951.62
5	9.88	0.13	1156.50	15.15	0.25	1160.85
6	9.04	0.09	1272.95	12.03	0.07	1272.91
7	18.21	0.39	1308.16	22.88	0.41	1305.06
8	13.35	0.22	1348.33	16.56	0.19	1347.97
9	9.03	0.15	1457.94	15.68	0.21	1454.91
10	12.71	0.51	1521.89	17.89	0.56	1519.56
11	16.58	1.00	1590.16	20.00	1.00	1589.12

Figure R9 (now added as Supplementary Fig. 41 in SI) | The comparison of Raman spectra of L5-Cu between OCP state and post reaction state.

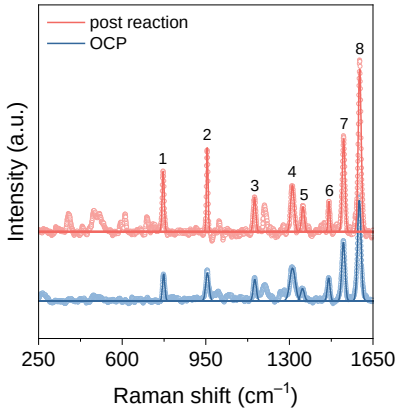

	OCP			Post reaction		
Peak No.	FWHM	Ratio	Wavenumber /cm^{-1}	FWHM	Ratio	Wavenumber /cm^{-1}
1	11.37	0.17	773.67	10.43	0.26	771.68
2	16.12	0.26	956.67	8.23	0.29	956.04
3	15.37	0.19	1155.30	12.46	0.18	1154.23
4	26.71	0.50	1313.11	17.37	0.33	1312.72
5	17.90	0.12	1354.76	13.67	0.14	1356.91
6	13.17	0.17	1464.47	9.31	0.11	1465.94
7	16.14	0.54	1526.20	13.75	0.53	1527.18
8	17.50	1.00	1592.77	14.90	1.00	1594.39

Figure R10 (now added as Supplementary Fig. 42 in SI) | The comparison of Raman spectra of L6-Cu between OCP state and post reaction state.

Reviewer #3:

The authors reviewed the paper very thoroughly and replied to all questions. I recommend this manuscript for publication. However, I have two points that should be re-visited first.

Reply: We sincerely thank this reviewer for the comments and suggestions which has helped improve the quality of this work.

Reviewer 3, Comment 5. Page 8, Line 17: The HOMO level...

Thanks for the clarification about the bonding of CO to Cu2+ and the additional citation (J. Am. Chem. Soc. 1985, 107, 578-584). Can the authors add this last sentence to the manuscript?

Reply: We have added "*CO bonds with Cu (orbital structure $Cu^{(2-\delta)+}$ ($[Ar]3d^{9+\delta}$)) through its 5σ orbital and π* orbital (i.e., back-donation) and the contribution share of each determines the overall binding strength (*J. Am. Chem. Soc.* 1985, 107, 578-584)" into the revised manuscript (page 13).

Reviewer 3, Comment 11.5: EXAFS model

Thanks for the re-work of the single-shell versus multiple-shell fit. The slight improvement of the fit possibly indicates that the shell is split, and 2-3 bond distances can be refined, which the authors have well demonstrated. However, the initial reviewer comment is still valid, in that neighboring-Z back-scatterers cannot be

distinguished. Therefore, the authors must clearly state that the assignment of N/O/C back-scatterers is subjective and is based on the prior knowledge of the structure, e.g. the interatomic distances are consistent with DFT.

The final fits (e.g. operando EXAFS) look really good, but there is a caveat. When making the model more detailed, e.g. by adding more shells and parameters, the errors of the individual parameters can increase significantly. Can the authors indicate errors for all the determined parameters, not only coordination numbers? Since the compounds here have a well-defined and well-known molecular structure, high errors are not a problem, and are more a measure of the sensitivity of the EXAFS technique itself. This should be briefly mentioned in the manuscript.

Reply: We have added the statement in the revised MS (page 6) "The assignment of N/O/C back-scatterers is subjective, and the interatomic distances are based on the structure simulated by DFT."

Besides, we have updated the errors for all the determined parameters of FT-EXAFS fitting (Tables R4–R8) and updated in SI.

Table R4 (now updated as Supplementary Table 1 in SI) | Interatomic distances and coordination numbers determined by EXAFS analysis of L2-Cu under OCP state before CO_2RR using L2-Cu model. Data range k = 2.5–11 Å^{-1}, amplitude reaction factor S_0^2 = 0.8, bond distance R = 0–4 Å. CN: Coordination numbers. ΔE: The inner potential shift. σ^2: The Debye-Waller factor. First shell: yellow lines; Second shell: blue lines; Third shell: green lines.

	Scatter path	CN	R (Å)	ΔE (eV)	σ^2 (Å^2)	R-factor
L2-Cu at OCP	Cu–O	2.00±0.06	1.83±0.12	1.2±0.4	0.00297±0.00371	0.64%
	Cu–N	2.00±0.06	1.99±0.01	1.2±0.4	0.00604±0.00386	
	Cu–N	2.05±0.23	2.88±0.07	1.2±0.4	0.01202±0.00585	
	Cu–C	2.03±0.21	3.16±0.15	1.2±0.4	0.0150±0.01146	
	Cu–C	1.02±0.11	3.35±0.24	1.2±0.4	0.03102±0.00644	
	Cu–Cu	2.06±0.33	3.11±0.27	1.2±0.4	0.00906±0.00411	
	Cu–C	1.02±0.12	3.22±0.19	1.2±0.4	0.03088±0.01241	
	Cu–N	1.02±0.11	3.37±0.36	1.2±0.4	0.02305±0.03155	
	Cu–N	1.01±0.09	4.09±0.25	1.2±0.4	0.02610±0.02044	
	Cu–C	2.02±0.20	4.28±0.37	1.2±0.4	0.02313±0.01972	

Table R5 (now updated as Supplementary Table 8 in SI) | Interatomic distances and coordination numbers determined by EXAFS analysis of L2-Cu at –0.69 V using L2-Cu model. Data range k = 2.5–11 Å^{-1}, amplitude reaction factor S_0^2 = 0.8, bond distance R = 0–4 Å. CN: Coordination numbers. ΔE: The inner

potential shift. σ^2: The Debye-Waller factor. First shell: yellow lines; Second shell: blue lines; Third shell: green lines.

	Scatter path	CN	*R* (Å)	ΔE (eV)	σ^2 (Å^2)	R-factor
–0.69 V	Cu–N	2.00±0.03	2.05±0.05	3.7±1.9	0.00907±0.00223	0.30%
	Cu–C	1.00±0.02	1.93±0.06	3.7±1.9	0.00791±0.00357	
	Cu–O	1.00±0.02	1.78±0.25	3.7±1.9	0.00514±0.00771	
	Cu–O	0.99±0.03	3.05±0.22	3.7±1.9	0.01910±0.00594	
	Cu–N	0.99±0.03	2.92±0.01	3.7±1.9	0.01492±0.00303	
	Cu–C	1.00±0.04	2.34±0.58	3.7±1.9	0.01487±0.00359	
	Cu–C	1.98±0.11	3.30±0.27	3.7±1.9	0.02531±0.00776	
	Cu–N	1.00±0.03	3.45±0.38	3.7±1.9	0.02918±0.00564	
	Cu–C	0.99±0.04	3.50±0.36	3.7±1.9	0.03207±0.00325	
	Cu–Cu	1.00±0.03	3.25±0.01	3.7±1.9	0.02085±0.00349	
	Cu–C	1.00±0.04	3.41±0.05	3.7±1.9	0.03777±0.01946	

Table R6 (now updated as Supplementary Table 9 in SI) | Interatomic distances and coordination numbers determined by EXAFS analysis of L2-Cu at –0.73 V using L2-Cu model. Data range k = 2.5–11 Å^{-1}, amplitude reaction factor S_0^2 = 0.8, bond distance R = 0–4 Å. CN: Coordination numbers. ΔE: The inner potential shift. σ^2: The Debye-Waller factor. First shell: yellow lines; Second shell: blue lines; Third shell: green lines.

	Scatter path	CN	*R* (Å)	ΔE (eV)	σ^2 (Å^2)	R-factor
–0.73 V	Cu–N	2.00±0.03	2.06±0.06	4.4±2.4	0.01410±0.00788	0.24%
	Cu–C	1.00±0.01	1.94±0.05	4.4±2.4	0.01089±0.00382	
	Cu–O	1.00±0.01	1.79±0.24	4.4±2.4	0.00630±0.00536	
	Cu–O	1.00±0.02	2.93±0.10	4.4±2.4	0.02093±0.01543	
	Cu–N	1.00±0.02	3.09±0.18	4.4±2.4	0.01932±0.00656	
	Cu–C	0.99±0.04	2.38±0.53	4.4±2.4	0.01038±0.00777	
	Cu–C	1.98±0.13	3.39±0.35	4.4±2.4	0.01953±0.00897	
	Cu–N	1.01±0.02	3.47±0.40	4.4±2.4	0.02127±0.01652	
	Cu–C	1.00±0.45	3.46±0.32	4.4±2.4	0.01568±0.00327	
	Cu–Cu	1.01±0.02	3.27±0.01	4.4±2.4	0.02247±0.01078	
	Cu–C	1.01±0.02	3.44±0.03	4.4±2.4	0.01650±0.00690	
	Cu–Cu	1.03±0.09	3.90±0.33	4.4±2.4	0.00650±0.00747	

Table R7 (now updated as Supplementary Table 10 in SI) | Interatomic distances and coordination numbers determined by EXAFS analysis of L2-Cu at –0.79 V using L2-Cu model. Data range k = 2.5–11 Å^{-1}, amplitude reaction factor S_0^2 = 0.8, bond distance R = 0–4 Å. CN: Coordination numbers. ΔE: The inner potential shift. σ^2: The Debye-Waller factor. First shell: yellow lines; Second shell: blue lines; Third shell: green lines.

	Scatter path	CN	R (Å)	ΔE (eV)	σ^2 (Å^2)	R-factor
–0.79 V	Cu–N	2.01±0.06	1.97±0.02	4.7±3.0	0.00501±0.00991	0.77%
	Cu–C	1.04±0.19	2.16±0.16	4.7±3.0	0.00248±0.00921	
	Cu–O	1.00±0.05	1.82±0.21	4.7±3.0	0.00358±0.00366	
	Cu–O	1.08±0.12	2.86±0.03	4.7±3.0	0.01793±0.00593	
	Cu–N	1.09±0.13	3.06±0.15	4.7±3.0	0.02924±0.00222	
	Cu–C	1.09±0.13	3.21±0.28	4.7±3.0	0.03324±0.03535	
	Cu–C	2.19±0.37	3.31±0.27	4.7±3.0	0.02514±0.00585	
	Cu–N	1.08±0.12	3.51±0.44	4.7±3.0	0.03591±0.00941	
	Cu–C	1.09±0.12	3.60±0.47	4.7±3.0	0.03693±0.00580	
	Cu–Cu	1.09±0.12	3.34±0.08	4.7±3.0	0.02749±0.00520	
	Cu–C	1.08±0.12	3.46±0.01	4.7±3.0	0.03816±0.00467	
	Cu–Cu	1.07±0.17	3.69±0.12	4.7±3.0	0.00985±0.00522	

Table R8 (now updated as Supplementary Table 11 in SI) | Interatomic distances and coordination numbers determined by EXAFS analysis of L2-Cu under OCP after CO_2RR using L2-Cu model. Data range k = 2.5–11 Å^{-1}, amplitude reaction factor S_0^2 = 0.8, bond distance R = 0–4 Å. CN: Coordination numbers. ΔE: The inner potential shift. σ^2: The Debye-Waller factor. First shell: yellow lines; Second shell: blue lines; Third shell: green lines.

	Scatter path	CN	R (Å)	ΔE (eV)	σ^2 (Å^2)	R-factor
OCP after reaction	Cu–O	2.00±0.05	1.82±0.13	1.2±1.3	0.00407±0.00675	0.57%
	Cu–N	2.00±0.06	1.99±0.01	1.2±1.3	0.00741±0.00635	
	Cu–N	2.02±0.20	2.87±0.08	1.2±1.3	0.01192±0.00750	
	Cu–C	2.03±0.16	3.22±0.22	1.2±1.3	0.02749±0.00735	
	Cu–C	1.01±0.07	3.28±0.17	1.2±1.3	0.02960±0.00648	
	Cu–Cu	2.03±0.16	3.10±0.28	1.2±1.3	0.01217±0.00671	
	Cu–C	1.02±0.14	3.05±0.36	1.2±1.3	0.01810±0.01012	
	Cu–N	1.01±0.07	3.37±0.36	1.2±1.3	0.03094±0.00464	
	Cu–N	1.01±0.08	4.11±0.26	1.2±1.3	0.02602±0.01044	
	Cu–C	2.02±0.17	4.29±0.37	1.2±1.3	0.02336±0.00552	

REVIEWERS' COMMENTS

Reviewer #2 (Remarks to the Author):

The authors have satisfactorily addressed all of my concerns in my previous review. I thank the authors for taking the time to add more quantitative details and precise phrasings that I think will be useful to the field.

Reviewer #3 (Remarks to the Author):

The reviewer comments are in my view well-addressed, and I recommend the paper for publication.

Response Letter

Reviewer #2:

The authors have satisfactorily addressed all of my concerns in my previous review. I thank the authors for taking the time to add more quantitative details and precise phrasings that I think will be useful to the field.

Reviewer #3:

The reviewer comments are in my view well-addressed, and I recommend the paper for publication.

Response: We are pleased that both reviewers recommended publication of our work. We would like to take this opportunity to thank the editor and all three reviewers for their invaluable feedback, which allows us to have significantly enhanced the quality of our work.